Understanding drivers and biases of simulated CO emissions from the INFERNO fire model over South America

Maria P. Velásquez-García[1,2], Richard J. Pope[1,2], Steven T. Turnock[3,4], Chetan Deva[1], David P. Moore[5,6], Guilherme Mataveli[7,8], Steve R. Arnold[1], Ruth M. Doherty[9], and Martyn P. Chipperfield[1,2]

[1]School of Earth and Environment, University of Leeds, Leeds, UK
[2]National Centre for Earth Observation, University of Leeds, Leeds, UK
[3]Met Office Hadley Centre, Exeter, UK
[4]Met Office@Leeds, University of Leeds, UK
[5]School of Physics and Astronomy, Space Park Leicester, University of Leicester, Leicester, UK
[6]National Centre for Earth Observation, Space Park Leicester, University of Leicester, Leicester, UK
[7]Earth Observation and Geoinformatics Division, National Institute for Space Research, São José dos Campos, Brazil
[8]Tyndall Centre for Climate Change Research, School of Environmental Sciences, University of East Anglia, Norwich, UK
[9]School of GeoSciences, University of Edinburgh, Edinburgh, UK

Correspondence: Maria P. Velásquez-García (eempvg@leeds.ac.uk)

Abstract. Integrating fire representation into climate models improves our understanding of ecosystem-fire-climate interactions by including connections between the carbon cycle and atmospheric composition. The Interactive Fires and Emissions algorithm for Natural Environments (INFERNO) is a new component of the UK Earth System Model (UKESM). Here, we evaluate carbon monoxide (CO) emissions from fires in South America as modelled by the INFERNO fire emissions model, which is coupled to the Joint UK Land Environment Simulator (JULES) in an offline configuration. Different satellite-based inventories were used for comparisons. To identify key factors driving simulated CO emissions and model-inventory biases, we use sensitivity experiments and a machine-learning approach. The findings indicate that INFERNO accurately capture the Arc of Deforestation in the southern Amazon as a primary source region of fire CO emissions, but it tends to overestimate these emissions by about 72%. The simulated emission patterns in this region are largely determined by drought conditions and Plant Functional Type (PFT), particularly tree fractions. Aligned, the experiments show a 100% increase in CO emissions in the southern Amazon region when using a drier meteorology dataset compared to the ERA5-based control run. In southern South America, INFERNO emissions, and in particular their seasonal cycle is affected by the tree PFT misrepresentation. The machine learning model explains 67% of the model-inventory biases using only model inputs, highlighting room for improvement and the need to consider additional factors. The machine learning model identified soil moisture and tree PFT as major contributors to the model bias. Future model development should focus on improving the representation of fuel moisture, fuel load, and human activities (e.g., agriculture and deforestation) in the fire model.

1 Introduction

Fires and their emissions can significantly impact our climate and ecosystems through complex land surface-fire-climate interactions. Annually, fires burn approximately 770 megahectares (Chen et al., 2023) and emit around 7.3 petagrams of CO_2 into the atmosphere (van der Werf et al., 2017), among other important greenhouse gases and air pollutants. As widely reported, the occurrence, propagation, and emissions of fires are strongly controlled by meteorological conditions and the type of vegetation present, even when fires are predominantly caused by human activity (Kelley et al., 2019; Forkel et al., 2019). In fact, fires are increasingly driven by climate change in our warming world (Liu et al., 2022b; Burton et al., 2024). Likewise, fire also influences climate and ecosystems by introducing feedbacks through atmospheric emissions (i.e. aerosols and greenhouse gases) and perturbations to the land surface. For instance, fire activity influences ecosystem competition, favouring fire-prone ecosystems over more sensitive ones, such as forested regions (Beckett et al., 2022). Furthermore, wildfire emissions can alter the biogeochemical cycles of key plant-growth elements, such as carbon, phosphorus, nitrogen, and iron (Bauters et al., 2018; Hamilton et al., 2022), leading to nutrient losses in burnt areas and increased nutrients in areas of deposition. Additionally, fire emissions (particularly aerosols) have strong direct and indirect impacts on climate through atmospheric scattering and cloud properties. Aerosols can suppress precipitation, driven by more cloud condensation nuclei (Wu et al., 2011; Thornhill et al., 2018), smaller drops and more evaporation and less convection provoked by a warmer cloud layer (Magahey and Kooperman, 2023; Thornhill et al., 2018; Wu et al., 2011). On a large scale, the most extreme wildfire emissions influence global circulation by altering the balance between the tropospheric and stratospheric radiation budgets (Zhou et al., 2020; Senf et al., 2023; Liu et al., 2005). The effect on the radiation balance can, in turn, influence ecosystems. For instance, in the Amazon forest, diffuse radiation enhanced by aerosols from fires increases plant growth (Rap et al., 2015). Overall, fires, ecosystems and climate are all strongly coupled, shaping the future evolution of all components involved.

Despite the clear importance of fire in the Earth's system, many Earth System Models, which model climate interactions, rely on prescribed data to represent fires and their emissions, leading to large uncertainties in future climate projections (Intergovernmental Panel on Climate Change (IPCC), 2023; Kloster and Lasslop, 2017; Hanan et al., 2022). When prescribed, although the effects of fires are parametrised, the fire feedback on the land surface is not represented. Multiple coupled models have attempted to represent the complex climate-fire-ecosystem interactions in the past few decades (Hantson et al., 2016). However, developing fully coupled fire models within global climate models is an active area of research with complex challenges still to overcome (Lasslop et al., 2019).

For the seventh Coupled Model Intercomparison Project (CMIP), the United Kingdom Earth System Model (UKESM) will couple the Interactive Fires and Emissions algorithm for Natural Environments (INFERNO) (Mangeon et al., 2016) to its land surface model (the Joint UK Land Environment Simulator - JULES) and atmospheric chemistry model (UK Chemistry and Aerosols Model - UKCA). INFERNO, coupled to JULES, has already participated in the Fire Modelling Intercomparison Project (FireMIP), where INFERNO provided an accurate representation of global burnt area and carbon emissions (Hantson et al., 2020; Teixeira et al., 2021). In FireMIP, INFERNO outperformed most of the studied coupled models in simulating the spatial patterns of fire carbon emissions (Hantson et al., 2020). However, the model has also faced challenges in representing

regional fire regimes across the world, including South America. Here, INFERNO's representation of fire properties has been limited by the complexity of socioeconomic and political influences on land management in the region (Burton et al., 2022). In general, FireMIP showed differences between models and a frequent overestimation of emissions in South America, where anthropogenic influences on fires (e.g., deforestation) are the main challenge (Li et al., 2019; Hantson et al., 2020). South America contributes around 15% of annual global fire carbon emissions and 40% of deforestation-related emissions (van der Werf et al., 2010), mainly due to deforestation in the Amazon. Changes in carbon balance and land cover in the Amazon can introduce significant regional and global impacts (Snyder, 2010; Zhou et al., 2020; Wang et al., 2023a). Moreover, parts of the Amazon have already become a substantial source of carbon due to deforestation and climate change (Gatti et al., 2021).

INFERNO has already been used to investigate a range of scenarios and events in South America (Burton et al., 2019, 2020), supported by global and specific performance evaluations (Burton et al., 2020; Hantson et al., 2020; Teixeira et al., 2021). However, previous studies have primarily focused on burnt area and carbon emissions from fires, whereas this study aims to evaluate the simulation of fire-derived emissions input into atmospheric models. Additionally, we seek to identify areas for development and improvement by analysing the biases associated with these emissions. For this, we compare the carbon monoxide (CO) emissions from fires simulated by JULES-INFERNO with various biomass burning inventories. To investigate key drivers factors controlling INFERNO CO emissions and their model-inventory biases, we used a sensitivity analysis and a machine learning approach.

2 Data and methods

2.1 Study area

This study assesses the spatial distribution, seasonality and temporal evolution of CO fire emissions in continental South America (a key global region for fire activity and emissions). We focus on three regions: Northern South America (North-SA), Central South America (Mid-SA), and Southern South America (South-SA), as shown in Fig. 1. These regions are designed to capture emissions from the main fire-active regions of South America, while also accounting for unique fire patterns. These regions are consistent with previous work that evaluated the ability of CMIP models' to simulate fire emissions, including assessing trends and biases, across South America (Li et al., 2024; van Marle et al., 2017). The North-SA region experiences a fire season because opposite to that of the southern region, due to the migration of the Intertropical Convergence Zone. The Mid-SA region encompasses fire emissions from the important Arc of Deforestation front (Pereira et al., 2022), an area threatened by continued land-use conversion and recognised as the world's largest savanna-forest transition (Marques et al., 2020). Importantly, defining Mid-SA as a broad but bounded region provides a practical scale for evaluating fire models like INFERNO, which are not designed for fine-scale simulations in highly variable zones such as the Arc of Deforestation. South-SA includes an important source of fire emissions from the Chaco biome. Although the division between Mid-SA and South-SA intersects the Cerrado fire-prone ecoregion, Mid-SA includes the deforestation front in the northern part of the Cerrado, where fires occur more frequently (Kim et al., 2025).

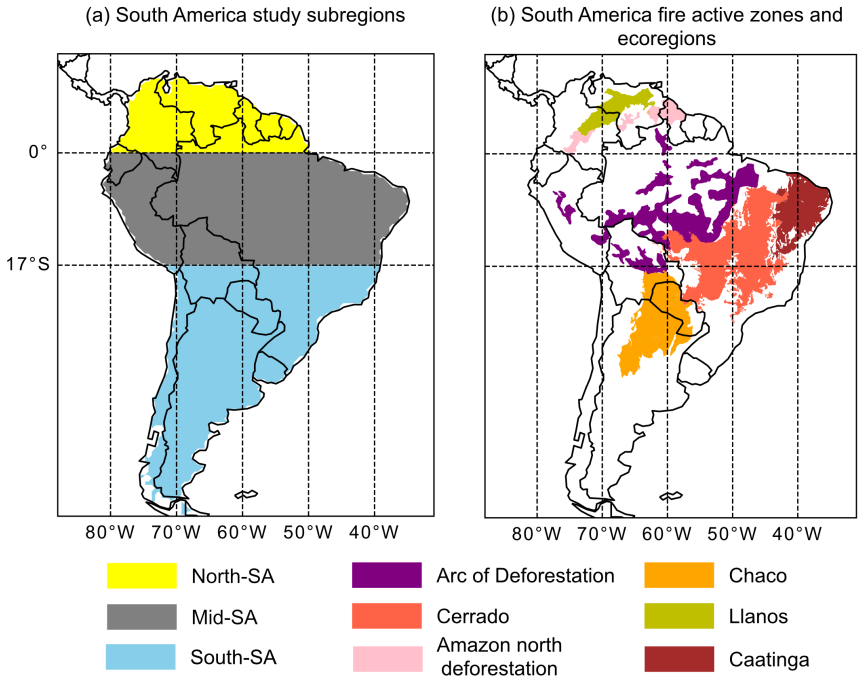

Figure 1. (a) Studied subregions and (b) assessed fire active zones and ecoregions in South America.

This study also assesses CO emissions from deforestation fronts and specific ecoregions of South America using the shapefiles provided by Pacheco et al. (2021) and Dinerstein et al. (2017), respectively. These zones are displayed in Fig. 1 (b). For the Arc of Deforestation, we used the deforestation fronts from Bolivia, Brazil, and Perú.

2.2 Biomass burning emission inventories

To evaluate the simulated CO emissions from fire, we utilised four biomass burning inventories. One of the key sources was the Global Fire Emissions Database (GFED), which is commonly used in modelling studies due to its extensive historical data and reliability. We specifically employed the GFED version 5 beta (GFED5) and version 4.1s (GFED4s) (van der Werf et al., 2017; Chen et al., 2023) to assess the consistencies/differences between them. Additionally, we incorporated the Global Fire Assimilation System version 1.2 (GFAS) (Kaiser et al., 2012) and the Brazilian Biomass Burning Emission Model (3BEM-FRP) (Pereira et al., 2022).

These inventories are based on two different fire products. GFED uses the burnt area as its primary satellite product, while GFAS and 3BEM-FRP rely on fire radiative power (FRP). GFED4s was the first GFED version to account for small fires by utilising the 500m MODIS bands (van der Werf et al., 2017). For GFED5, efforts to include small fires continued, incorporating corrections based on Landsat and Sentinel-2 observations (Chen et al., 2023). GFAS exploits real-time emissions estimates using the MODIS near-real-time FRP product (Kaiser et al., 2012). Similarly, 3BEM-FRP utilises FRP data from MODIS,

although it is not a near-real-time product. 3BEM-FRP uses an adjustment factor to account for fires that exceed the spatial and temporal resolution of MODIS FRP based on hotspots from VIIRS and the geostationary satellites GOES and SEVIRI (Pereira et al., 2022).

The estimates of CO emissions from these inventories vary substantially because each one calculates the amount of burnt dry matter differently (Hua et al., 2024). However, they all follow the same approach in converting this burnt matter into emissions using emission factors (EF) [$g\,kg^{-1}$] that vary by land use and land cover. The EFs are commonly taken from Akagi et al. (2011) and Andreae and Merlet (2001). This consistency in the factor is particularly evident for CO, where EFs are consistent across different inventories (Liu et al., 2020; Hua et al., 2024). GFASvn1.2 and 3BEM-FRP also use a combustion factor to determine the amount of biomass burnt at different FRP energy levels. For this, they rely on external products, GFEDv3.1 for GFAS and the Fire Energetics and Emissions Research v1 (FEERv1) for 3BEM-FRP (Kaiser et al., 2012; Pereira et al., 2022).

GFAS and 3BEM-FRP were downloaded daily with a spatial resolution of $0.1^\circ \times 0.1^\circ$, while GFED5 and GFED4s were downloaded with a monthly resolution and a spatial resolution of $0.25^\circ \times 0.25^\circ$. All of the inventories were resampled to a monthly temporal resolution and a spatial resolution of $0.5^\circ \times 0.5^\circ$ to match the model output dimensions in the JULES-INFERNO configuration (Section 2.3).

For the machine learning analysis of INFERNO biases (Section 2.6) and for visualising differences in selected figures, we calculated an ensemble average (mean) dataset based on the four inventories: GFED4s, GFED5, GFAS, and 3BEM-FRP. Each inventory was equally weighted in the average. GFED4s and GFAS are well-established inventories in the literature. While they have outperformed other inventories in their emissions estimate in South America (Hua et al., 2024; Reddington et al., 2019), their biases have also been noted (Naus et al., 2022; Liu et al., 2020). In contrast, 3BEM-FRP and GFED5 (the beta version) are considered next-generation inventories. They have been adjusted to better represent small fires and include updated and more accurate land cover data (Mataveli et al., 2023). However, these newer inventories lack the extensive long-term validation that GFED4s and GFAS have undergone. Overall, using an average of these inventories represents a balance between incorporating innovative methodologies and relying on well-established datasets for this study.

2.3 JULES-ES setup

We used the JULES-ES configuration from the historical run of the third simulation round of the Inter-Sectoral Impact Model Intercomparison Project (ISIMIP3a) (Mathison et al., 2023), as it features a recent setup comparable to JULES in UKESM. The JULES-ES setup uses a $0.5^\circ \times 0.5^\circ$ latitude–longitude grid. While JULES can be run for several centuries for climate applications, in this study, we ran JULES-ES from 2001 (study period of 2004-2021) to match the satellite era over the past few decades.

ISIMIP3a includes a core of experiments based on climate-related forcings and direct human forcings (Frieler et al., 2024). For climate-related forcings and for the more recent period (from around 1980), the project includes three optional observation-based meteorological datasets: W5E5, ERA5, and 20CRv3. The W5E5 data ends in 2019, 20CRv3 ends in 2015, and ERA5 ends in 2021 (Frieler et al., 2024). In our study, we used ERA5 for the control analysis since it encompasses the entire study period (2004 - 2021). The other two datasets were utilised for the flammability sensitivity experiments described in Section

2.4. The human-forcing datasets in ISIMIP3a prescribe land-use (agricultural and pasture fractions), population density, and nitrogen deposition.

For this setup, JULES-ES includes 13 plant functional types (PFTs), which include nine natural and four managed PFTs (Mathison et al., 2023). The natural PFTs are Broadleaf Deciduous Trees, Tropical Broadleaf Evergreen Trees, Temperate Broadleaf Evergreen Trees, Needleleaf Evergreen Trees, Needleleaf Deciduous Trees, Evergreen shrubs, Deciduous shrubs and C3 and C4 Grasses. The managed PFTs are C3 and C4 Crops and Pastures. C3 and C4 refer to photosynthetic pathways. C4 plants are adapted to high temperatures and light intensities, reducing water loss and improving CO_2 fixation under these conditions compared to C3 plants. JULES-ES also contains four non-vegetation land covers (bare soil, lake, ice, urban). The PFTs are simulated globally within JULES-ES using the dynamic global vegetation model (DGVM) TRIFFID (Top-down Representation of Interactive Foliage and Flora Including Dynamics), which represents PFT competition and their biomass (Burton et al., 2019).

2.3.1 INFERNO

The INFERNO fire model was developed by Mangeon et al. (2016) and simulates the burnt area (BA_{PFT}) based on simulated ignitions (I_T) and flammability (F_{PFT}), as described by Equation 1. The BA_{PFT} is scaled by PFT using the factor called average burnt area ($\overline{BA_{PFT}}$), which describes the minimum scar of burnt area per PFT.

$$BA_{PFT} = I_T \, F_{PFT} \, \overline{BA_{PFT}} \tag{1}$$

I_T is composed of natural and anthropogenic ignitions (I_N and I_A), which are calculated using the lightning rate and population density (PD), respectively. As Equation 2 shows, I_T is further scaled by a factor representing fires not suppressed by humans (f_{NS}). The I_N is equal to 75% of cloud-to-ground lighting per km^2 in a month. The seasonal lighting cycle is prescribed into the model. Both I_A and f_{NS} are used in Equations 3 and 4. The Human Development Index (HDI) is also used in the two equations, as a further development of INFERNO added by Teixeira et al. (2021). For this study, we are using HDI=0 in most of the analyses; however, we include HDI in a sensitivity experiment (Section 2.4).

$$I_T = (I_N + I_A)\frac{f_{NS}}{8.64 \times 10^{10}} \tag{2}$$

$$I_A = k_{(PD)} \, PD\alpha \times (1 - HDI) \tag{3}$$

$$f_{NS} = 7.7(0.05 + 0.9 \times e^{-0.05PD}) \times (1 - HDI) \tag{4}$$

As described in Equation 5, F_{PFT} depends on the relative humidity (RH) in %, precipitation rate (*R*) in mm day^{-1} and temperature in K from the prescribed input meteorological dataset. The land surface model, JULES, provides the inputs of soil moisture content (θ) as a fraction of saturation. JULES also pass the leaf carbon and decomposable plant material [kg m^{-2}], which are used to calculate the fuel load index (FL). The prescribed temperature is used to calculate the Goff-Gratch saturation vapour pressure (α), further explained in Mangeon et al. (2016).

$$F_{PFT} = \begin{cases} 1 \quad \text{for} \quad RH < RH_{low} \\ \alpha \frac{RH_{high} - RH}{RH_{high} - RH_{low}} e^{-2R} FL_{PFT}(1-\theta) \quad \text{for} \quad RH_{low} \leq RH \leq RH_{high} \\ 0 \quad \text{for} \quad RH > RH_{high} \end{cases} \tag{5}$$

For Equation 5, RH_{low} = 10 % and RH_{high} = 90 %. These are used to scale the influence of RH from 0 to 1. Consequently, F_{PFT} ranges from 0 to 1.

The emitted carbon (EC_{PFT}) is calculated based on BA, the available carbon (C_i) and the combustion completeness (CC) for wood and leaves. This final term describes the minimum and maximum carbon fractions burnt during fire events and can be defined depending on PFT. However, in this study these are defined as $CC_{min,leaf} = 0.8$, $CC_{max,leaf} = 1$, $CC_{min,wood} = 0.0$ and $CC_{max,wood} = 0.4$ regardless of PFT following Mangeon et al. (2016). Equation 6 defines the EC_{PFT}.

$$EC_{PFT} = BA_{PFT} \times \sum_{leaf,wood}^{i} (CC_{min,i} + (CC_{max,i} - CC_{min,i})(1-\theta))C_i \tag{6}$$

The emission of CO is described by Equation 7, which includes the EC_{PFT} and the EF for CO for each PFT ($EF_{CO,PFT}$).

$$E_{CO,PFT} = EC_{PFT}\, EF_{CO,PFT}/[C] \tag{7}$$

In this equation, [C] describes the dry carbon fraction, assumed to be 50% (Mangeon et al., 2016).

Table S1 presents the $\overline{BA_{PFT}}$ and EF for each PFT modelled. The EF_{CO} from C3-Crop and C4-Crop were not included in this model setup of JULES, which did not account for the crop PFTs. However, we conducted an experiment to assess the impact of fire CO emissions from crops. The experiment showed that excluding crops from simulations produced a negligible change in CO emissions across South America, increasing simulated CO emissions by only 1.4% for South-SA when included (see Fig. S1). However, it is important to note that INFERNO does not model crops differently from other PFTs; meaning that harvesting periods and crop seasonality are not included or represented. In this study, we do, however, evaluate the contributions of the crops' PFT fractions to the model biases (see Section 2.6).

2.4 Sensitivity experiments on INFERNO

We conducted multiple experiments to assess the sensitivity of various processes and parameters controlling simulated fire emissions, and their roles in the INFERNO response. We did this using a one-at-a-time technique, varying individual parameters and variable inputs from the control simulation described in Section 2.3.1. The experiments are briefly summarised in Table 1. We evaluated the role of anthropogenic and natural ignition in different scenarios. First, we simulated total ignition with a constant global anthropogenic ignition rate of 1.5 ignitions/km^2/month, based on GFED estimates (Mangeon et al., 2016). For this, only I_N varies in Equation 2, which we label IT-NAT. The role of both I_A and I_N was further evaluated by using a scenario with constant magnitudes for both ignitions; 1.5 ignitions/km^2/month for I_A and 2.7 flashes/km^2/yr for I_N. This experiment is labelled IT-CST. We also analyse socioeconomic scaling in ignition using the HDI as suggested by Teixeira et al.

(2021). This experiment directly influences anthropogenic ignitions and fire suppression. The HDI was incorporated into the model using the dataset provided by Kummu et al. (2018). The experiment is labelled IT-HDI.

To analyse the role of the meteorological conditions and the uncertainty it can introduce into the simulations, we use different meteorological datasets from the ISIMIP3a climate-forcing dataset. In this, we compared the ERA5-based control with the simulations using W5E5 and 20CRv3. These experiments are named as F-W5E5 and F-20CR, respectively. Notice that, in addition to flammability in Equation 5, the meteorological conditions also affect EC_{PFT} in Equation 6 through the carbon soil moisture and the available carbon.

Table 1. Description of the sensitivity analysis experiments on INFERNO

Short name	Direct impacted process	Description
Control		Vary ignitions and ERA5 meteorology
IT-CST	Ignition	Use constant both I_A and I_N ignition
IT-NAT		Use constant I_A and vary I_N ignition
IT-HDI		Include HDI at country level
F-W5E5	Flammability and emitted carbon	Prescribed W5E5 meteorology
F-20CR		Prescribe 20CRv3 meteorology
CC-VAR	Combustion	Vary CC across PFTs
CC-DEL		Remove the constraint brought by CC to burnt carbon
BA-CST	Burnt area	Use constant $\overline{BA}$ regardless of PFT
EF-CST	Emission Factor	Use constant EF regardless of PFT
NO-FDBK	Feedback	Decouple INFERNO-JULES feedback
PFT-OBS	Plant Functional Type	Prescribe observational-based PFTs

We also investigate the impact of factors such as $\overline{BA_{PFT}}$, $EF_{CO,PFT}$ and CC on simulated CO. For $\overline{BA_{PFT}}$ and $EF_{CO,PFT}$, we used two experiments, one with constant $\overline{BA}$ and the other with constant EF_{CO}. These experiments also provide information on the effect of PFTs on the factors. These are labelled as BA-CST and EF-CST, and for these we respectively used 0.8 km^2 fire^{-1} for $\overline{BA}$ and 78 $g\,kg^{-1}$ dry matter for EF_{CO}. Regarding the combustion completeness factors, we ran two experiments. For the first, CC-VAR, we used literature-based values for $CC_{min,leaf}$ and $CC_{max,wood}$, which vary across PFTs (van Leeuwen et al., 2014) (see Table S1). For this experiment, We did not modified $CC_{max,leaf}$ and $CC_{min,wood}$, so this was set as 1 and 0 as in the control run. For the second experiment, we used a scenario with CC_{min} and CC_{max} set as 0 and 1 for both leaf and wood. As a result, CC is removed from Equation 6 and the EC_{PFT} will then depend on a unconstrained soil moisture to calculate how much carbon from leaf and wood is simulated to be burnt. This experiment is named CC-DEL, as the emission calculations are now effectively independent of CC in INFERNO.

Additionally, for the sensitivity analysis, we included a prescribed PFT experiment, PFT-OBS, to evaluate the performance and sensitivity of the model to a different and more accurate PFTs. For this, we used an annual-resolution PFT dataset generated

by the ISIMIP3a team (Mathison et al., 2023) based on the work of Harper et al. (2023), and the Land-Use Harmonisation dataset provided for ISIMIP3 (Volkholz and Ostberg, 2022). This dataset covers the study period only through to 2019, so 2020 and 2021 used the same PFT fractions as 2019. Finally, we wanted to evaluate the scale of INFERNO feedback in its own simulation using a no-feedback scenario, labelled NO-FDBK. In this experiment, the outputs from INFERNO are not passed to JULES or TRIFFID. Therefore, in NO-FDBK, INFERNO does not contribute to carbon losses and PFT perturbation and competition. These processes are parametrised instead (Burton et al., 2019).

2.5 CO emissions variability and comparison

2.5.1 Mean relative range

We use the mean relative range (Range%) to quantify the average variation in estimated annual CO emissions across inventories for a specified region or zone. To calculate the Range%, we first computed the annual range of total CO emission estimates (y) for the area for each year i in the study period, defined as the difference between the maximum and minimum values across inventories. These ranges are then normalised by dividing them by the average emission magnitude across the inventories for each year. The resulting values are averaged over the entire study period (of length N) and multiplied by 100 to express the Range% as a percentage, as described by Equation 8.

$$Range\% = \frac{100}{N}\sum_{i}^{N}\frac{max(y_i) - min(y_i)}{\overline{y_i}} \tag{8}$$

Range% is designed to inform about the spread of estimated CO emissions magnitudes, considering the wide range of results from satellite-based estimations. The metric is used only to investigate inventory ranges and is not applied to INFERNO in this study.

2.5.2 Trend CO emissions calculation

We use CO emissions trends to assess the temporal evolution of CO emissions from inventories and INFERNO. To calculate the trends, we use the ordinary least squares linear regression (Perktold et al., 2024). This returns absolute trend values ($Ggyr^{-2}$), which we express as a percentage relative to the intercept (i.e., representing CO emissions at the start of the assessment period). We quantified the statistical significance of the CO emissions trend derived from both the inventories and INFERNO using the Mann-Kendall test at the 95% confidence level (Hussain and Mahmud, 2019). The trend and its significance were calculated separately for the individual grid point data and the regional cumulative emissions based on annual CO emissions.

2.5.3 Percentage mean bias

We utilised the percentage mean bias (Bias%) to assess the model's CO emissions biases related to spatiotemporal variations, seasonal cycles, and trends. As given by Equation 9, this metric calculates the average difference between a set of gridded values

from the model (denoted as x) and a corresponding set of gridded observational values (denoted as y). The observational values are used to scale these differences.

$$Bias\% = \frac{Mean(\mathbf{x}-\mathbf{y})}{Mean(\mathbf{y})} \times 100 \quad (9)$$

In Equation 9, x and y refer to different variables depending on the Bias% to be calculated. For the spatiotemporal Bias%, x and y denote the annual CO emissions and are defined on time-latitude–longitude coordinates. Conversely, for the seasonal cycle Bias%, x and y indicate the gridded seasonal cycle amplitude. The amplitude is determined by subtracting the mean of three consecutive months centred on the month of y maximum emissions from the average magnitude of the remaining months. Finally, for the trend Bias%, x and y correspond to the gridded trend of CO emissions from 2004 to 2021, which are calculated as explained in Section 2.5.2. For the seasonal cycle and trend Bias%, x and y are defined on latitude–longitude coordinates.

As this metric was also implemented for the sensitivity analysis, x magnitudes were replaced with the corresponding information from every sensitivity experiment run (described in Section 2.4). While y magnitudes were replaced by the control run data.

2.6 Machine learning for INFERNO CO emission biases explainability

Similar to other studies (Hess et al., 2023; Liu et al., 2022a), we utilised machine learning to identify the key factors causing annual biases in CO emissions and their potential contributions to mitigate these biases. Specifically, we calculated the annual biases of INFERNO by subtracting the average annual emissions estimated by the inventories from the total annual emissions simulated by INFERNO. Our target variable consisted of annual pixel-scale biases. The primary objective of our analysis was to identify the key factors contributing to these biases and determine whether the INFERNO inputs (both prescribed and modelled variables) were sufficient to explain them at this scale. For this analysis, we utilised a gradient-boosting framework implemented using the Python library XGBoost (Chen et al., 2025).

We chose 20 inputs from INFERNO to use as features for the machine learning model. These comprised prescribed data and JULES outputs used by INFERNO to calculate emissions. These are: population density, lightning flash rates, precipitation rate, relative humidity, temperature, soil moisture, HDI, wood carbon, leaf carbon and 11 PFTs. All PFTs were considered; however, Needleleaf Deciduous Trees and Needleleaf Evergreen Trees were merged to a single Needleleaf Trees PFT, and Evergreen Shrubs and Deciduous Shrubs were merged to a single Shrub PFT. Soil moisture, wood carbon, leaf carbon, and PFTs were directly taken from JULES simulations. The other variables were obtained from the original datasets prescribed as inputs to INFERNO. The inputs to the machine learning model are the gridded datasets resampled to an annual resolution for the study period (2004 to 2021). We enable correlated features in the machine learning model, as in a gradient boosting model, any redundant information is automatically disregarded. This happens because the decision trees are built by splitting features in a series of dependent trees, so they can not make identical splits using correlated features (Power et al., 2024).

The dataset was randomly partitioned into training (80%) and testing (20%) subsets within a five-fold cross-validation framework. This strategy helps ensure that model performance is evaluated independently of any single training–testing split,

reducing the risk of overfitting and improving generalizability. We ran hyperparameter tuning to select the hyperparameters that lead to the best model performance. This was conducted using a random search method on each training set in a five-fold cross-validation. We used Sklearn's RandomizedSearchCV function with 500 iterations (i.e., n_iter=500) (Pedregosa et al., 2011). The model's performance was evaluated using the coefficient of determination (R^2), which indicates how much of the variability in the target CO emission biases is captured by the XGBoost model. Additionally, the Root Mean Square Error (RMSE) and Mean Absolute Error (MAE) measure the average difference between the predicted and actual values, with Root Mean Square Error being more sensitive to outliers.

Since the objective was to identify the key factors contributing to biases in CO emissions from INFERNO, special attention was given to the feature-contribution methodology. We employed the Shapley additive explanations (SHAP) method using the Python package from Lundberg et al. (2020). SHAP is based on cooperative game theory and measures each feature's contribution to each prediction by calculating SHAP values. These values are calculated using a weighted average of the differences in predictions when the feature is added to all possible subsets of the remaining features (Lundberg et al., 2020). We have used SHAP values to explain the dominant drivers in fire emissions in a consistent way with other recent studies, which also exploit machine learning methods for wildfire result applications (Wang et al., 2023b, 2022; Liu et al., 2024). SHAP values are computed for every prediction in the test set for every iteration of the five-fold cross-validation process.

We utilise two additional features to assess the SHAP values: the first feature categorises the pixels into North-SA, Mid-SA, and South-SA, while the second feature identifies a pixel's location on a map. With this, we can describe SHAP values based on their geographical location. These extra features were only used after calculating the SHAP values, so they were not used to train the model. To calculate the dominant feature at each pixel, we identify the feature with the largest positive or negative SHAP value, and we consistently assign it to pixels with an average positive or negative CO emission bias. Once we established the most important feature for each pixel across the years, we calculated the mode to identify which feature consistently contributes the most.

3 Results

3.1 Estimated and modelled fire CO emissions in SA

The Arc of Deforestation accounts for around 40% of the annual fire CO emissions in South America. Figure 2 demonstrates the extent to which the inventories are able to represent the substantial CO emissions source from the deforestation front. Here, INFERNO generally captures the broad-scale features of emissions from this source, including its latitude-longitude range. This level of performance in relation to inventories is typical in global fire models like INFERNO. This is due to the inherent challenges in simulating a stochastic process, such as ignition, at a detailed scale using only vegetation data, meteorological information, and population density (Rovithakis et al., 2025). Therefore, simulating fine-scale features in a variable region, such as the Arc of Deforestation, are outside the scope of INFERNO. On this deforestation front, the PFTs appear to drive the spatial distribution of CO emissions in the INFERNO simulations, using the relative abundance of Broadleaf Deciduous Trees and Tropical Broadleaf Evergreen Trees. However, the large area of emissions results in a general overestimation of

CO emissions where Tree PFTs dominate. INFERNO overestimates CO emissions in Mid-SA with a spatiotemporal Bias% of around 72% (see Table 2).

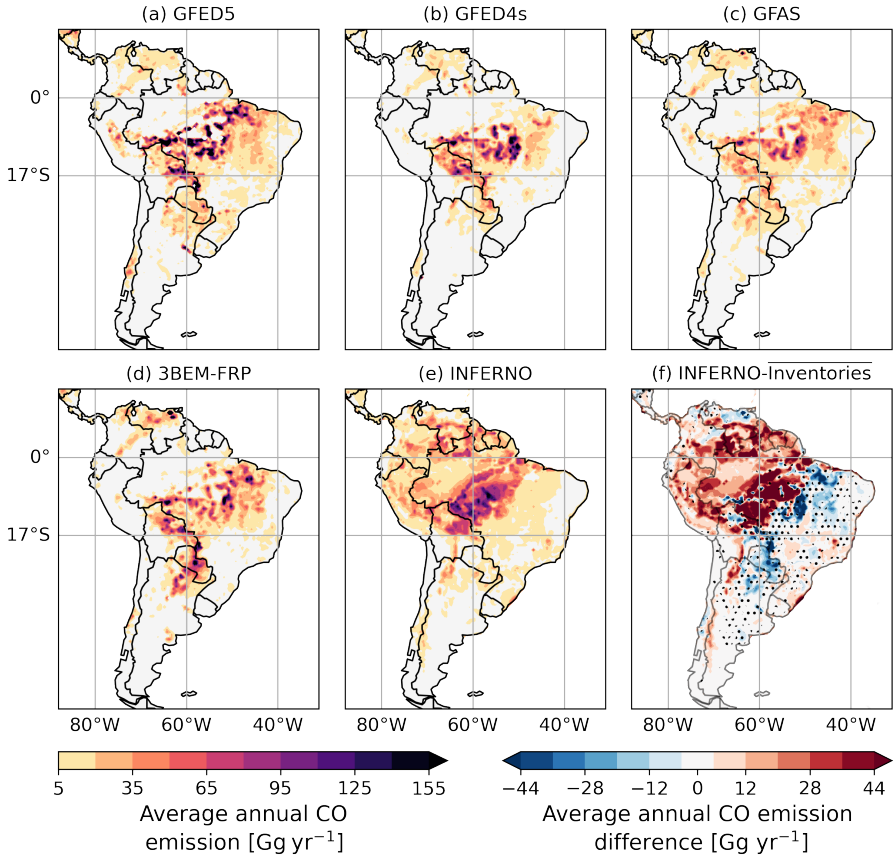

Figure 2. Annual mean fire CO emissions for 2004-2021 estimated by (a) GFED5, (b) GFED4s, (c) GFAS, (d) 3BEM-FRP, and simulated by (e) INFERNO. (f) shows the absolute differences between the INFERNO simulated and the average estimate of fire CO emissions. The areas hatched with dots in (f) indicate where the simulated and estimated emissions are statistically similar according to the Mann-Whitney test; this applies only to areas with nonzero emissions from at least one part.

The Arc of Deforestation demonstrates challenges not only for INFERNO, but also for the inventories, whose annual estimates have a Range% of 84% in the deforestation front. Liu et al. (2020) highlights small fires and surface obscuration due to cloud or haze as important sources of uncertainty in the estimations for this region. Here, GFED5 estimates the highest annual total fire CO emissions (37.0 $Tg\,yr^{-1}$). In contrast, GFED4s, GFAS, 3BEM-FRP estimate emissions of 21.1 $Tg\,yr^{-1}$, 19.0 $Tg\,yr^{-1}$ and 21.2 $Tg\,yr^{-1}$ respectively, which are approximately 40% of GFED5 estimates.

The Mid-SA region also includes the deforestation front in the Cerrado ecoregion, a fire-prone ecosystem with a mix of grasslands, shrublands, and forests. The inventories agree on estimating CO emissions of around 9.3 $Tg\,yr^{-1}$ (Range%:42%). In this context, the INFERNO estimation of 7.5 $Tg\,yr^{-1}$ falls within the interquartile range of estimates from most invento-

ries. In contrast to the Arc of Deforestation, INFERNO incorporates more of the relevant elements to simulate the fire-prone nature of the Cerrado, which can be highly dependent on both vegetation and meteorological conditions, even when it is also influenced by anthropogenic activity.

Together, North-SA and South-SA account for approximately 25% of annual CO emissions in South America, and both regions contain hotspots of particular interest. In North-SA, the fire-prone Llanos ecoregion, a mosaic of grasslands and savannas between Colombia and Venezuela, contains around 35% of the region's annual fire CO emissions according to most of the inventories, except for 3BEM-FRP, which estimates 58% of the annual emissions. The CO emissions estimates have a Range% of 33%. In the Llanos ecoregion, INFERNO simulates emissions to be within the inventory's range (2.1 $Tg\,yr^{-1}$); however, for the model, this is only 10% of total North-SA emissions. This is because in North-SA, INFERNO inaccurately simulates higher emissions from areas dominated by Tree PFTs (see Fig. S2). Consequently, the CO emissions simulated by INFERNO in North-SA are 2 to 4 times higher than those shown in the inventories (see Table 2).

In South-SA, the Chaco ecoregion contributes around 37% of fire CO emissions to the region according to most of the inventories, except for 3BEM-FRP, which estimates a contribution of around 54% (9.4 $Tg\,yr^{-1}$). The high CO emissions from 3BEM-FRP were previously linked to the combustion factor used in the inventory based on FEERv1.0 (Pereira et al., 2022). The Range% magnitudes for the Chaco ecoregion, including and not including 3BEM-FRP, are 124% and 55%, respectively. In this ecoregion, INFERNO estimates lower annual CO emissions than the inventories (2.3 $Tg\,yr^{-1}$). The model only falls with the GFED4s annual emission interquartile range as this inventory is substantially lower than the others in this ecoregion (see Fig. 2). This particular ecoregion is not well represented by TRIFFID either, which simulates higher proportions of C4 Grasses to be the dominant PFT, whereas more satellite-informed datasets describe the dominant PFT as Broadleaf Deciduous Trees (see Fig. S2). Despite not capturing the active fire zone for South-SA, INFERNO annual CO emissions are within the range of CO emissions estimated by the inventories. Here, the CO emissions are balanced by the overestimation in the Temperate Broadleaf Evergreen Tree-dominated region in the Andean mountains.

In general, the annual CO emissions estimates from the inventories for Mid-SA and North-SA have a Range% of 102% and 196%, respectively, indicating lower agreement between the inventories than for South-SA (Range%=76%). Conversely, INFERNO has the highest absolute spatiotemporal Bias% in North-SA (285%). The inventories differ on whether INFERNO, on average, overestimates or underestimates emissions in South-SA (see Table 2).

3.1.1 Seasonal cycle of fire CO emissions in South America

South America has a distinct seasonal cycle in fire activity, represented spatially in Fig. 3 (a) and (b) with the timing of the emissions peak, and by Fig. 3 (c),(d),(e) with the average monthly CO emissions. The emissions show high fire activity from August to October in Mid-SA and South-SA, and from January to April in North-SA. As expected, the inventories tend to differ greatly during the fire-active period, leading to the annual differences discussed above. However, the differences between them remain consistent over time, allowing the inventories to exhibit a high correlation in their monthly total CO emissions ($R > 0.9$) at the regional scale (see Fig. S3). Although INFERNO monthly CO emissions do not capture the desired seasonal cycle across the three regions analysed, the monthly total emissions still show a strong correlation with the inventories ($R > 0.73$).

Here, INFERNO is persistently higher than the inventories in non-fire seasons (see Fig. 3), and thus over-predicts background fire activity.

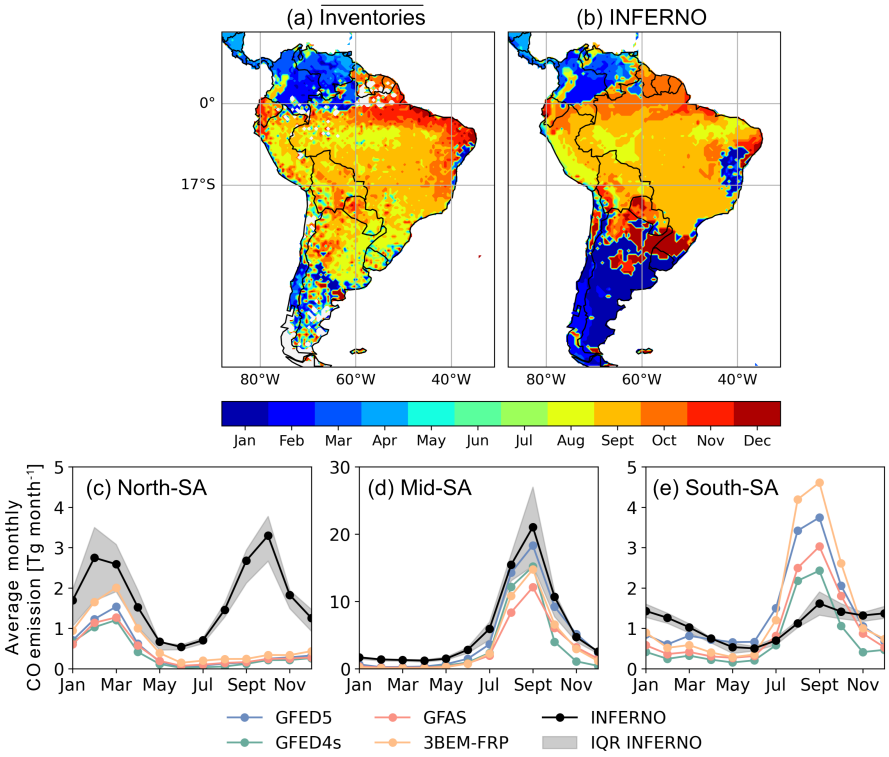

Figure 3. CO emissions peak timing across South America based on the (a) average estimates of CO emissions and (b) INFERNO CO emission simulations, and the average seasonal cycle of the estimates and simulated CO emissions for (c) North-SA, (d) Mid-SA and (e) South-SA. The shading in panels (c), (d) and (e) illustrate the inter-quartile range (IQR) of INFERNO monthly emissions.

Figure 3 (d) highlights how INFERNO simulates a seasonal cycle peaking in September, similar to the inventories for Mid-SA. Within the inventory range, the GFED5 average seasonal cycle sits within the INFERNO interquartile range. In fact, between August and October, INFERNO and GFED5 show similar distributions (i.e., not significantly different). However, outside this period, INFERNO total monthly emissions are larger than all of the inventories. Spatially, Fig. 3 shows that INFERNO manages to simulate the timing of the CO emission peaks for the fire-active areas in Mid-SA; the absolute Bias% in the seasonal cycle amplitude is less than 10% compared to most of the inventories (see Table 2), except for comparison with GFED5. The GFED5 dataset exhibits a large seasonal cycle, particularly across the Arc of Deforestation, which contributes to higher average amplitudes.

Figures 3 (c) and (e) show that INFERNO inaccurately represents the seasonal cycle in both North-SA and South-SA. For North-SA, the peak period of fire activity is represented, but with magnitudes higher than any of the inventories for January to April. Additionally, INFERNO simulates an erroneous second peak of emissions in October with similar magnitudes to the

Table 2. Total annual fire CO emission average magnitudes, seasonal cycle amplitudes and trends for North-SA, Mid-SA and South-SA and INFERNO Bias% in these metrics compared with inventories.

Item		GFED5	GFED4s	GFAS	3BEM-FRP	INFERNO
CO emission [$Tg\ yr^{-1}$]						
North-SA	Mean (SD)	5.5 (2.0)	4.4 (1.8)	5.0 (1.3)	13.1 (4.4)	21.0 (3.6)
	INFERNO Bias%	279	382	317	164	0
Mid-SA	Mean (SD)	56.6 (23.1)	37.2 (20.3)	35.2 (17.1)	39.9 (19.5)	70.2 (15.8)
	INFERNO Bias%	24	89	99	76	0
South-SA	Mean (SD)	16.8 (4.9)	8.7 (4.0)	11.8 (2.7)	17.4 (6.4)	13.1 (1.2)
	INFERNO Bias%	-22	50	11	-25	0
Seasonal cycle amplitude [$Tg\ yr^{-1}$]						
North-SA	Amplitude (SD)	0.9 (0.6)	0.7 (0.5)	0.8 (0.4)	1.2 (0.7)	0.7 (0.9)
	INFERNO Bias%	11	45	39	9	0
Mid-SA	Amplitude (SD)	12.3 (5.8)	9.8 (6.0)	7.9 (4.3)	9.8 (5.6)	13.2 (4.5)
	INFERNO Bias%	-31	1	9	-6	0
South-SA	Amplitude (SD)	2.2 (0.9)	1.6 (1.0)	1.9 (0.7)	3.1 (1.5)	0.4 (0.2)
	INFERNO Bias%	-82	-72	-78	-84	0
Trend 2004-2021 [% yr^{-1}]						
North-SA	Trend (confidence)	2.7 (-1.4,6.9)	2.7 (-2.2,7.7)	1.0 (-1.6,3.6)	**5.9 (1.5,10.4)**	0.8 (-1.0,2.6)
	INFERNO Bias%	21	28	50	23	0
Mid-SA	Trend (confidence)	**-3.0 (-5.6, -0.4)**	-2.5 (-6.5, 1.6)	**-3.9 (-6.4, -1.5)**	-3.2 (-6.3, -0.1)	1.6 (-0.8, 4.0)
	INFERNO Bias%	30	20	53	27	0
South-SA	Trend (confidence)	-0.8 (-3.5,1.8)	3.0 (-2.5,8.5)	-0.9 (-2.9, 1.1)	1.6 (-2.4, 5.7)	**-0.4 (-1.3, 0.4)**
	INFERNO Bias%	-9	-24	-8	-10	0

Note: The magnitudes of trends are highlighted in bold when the Mann-Kendall test indicates a significant trend at the 95% confidence level (p-value$\leq$0.05). Regionally aggregated annual CO emission time series are used for the temporal trend analysis. In the table, 'SD' and 'confidence' refer to the standard deviation values and the 95% confidence intervals. Notice that all Bias% are calculated based on gridded magnitudes (see Section 2.5.3), while the magnitudes of the metrics are based on total CO emissions for the regions.

first peak. Although emissions in the Tree PFT domain to the east of the region tend to peak in October (Cummings et al., 2025) (see Fig. S3), these are negligible compared to the regional emissions around March. Furthermore, as this is the second rainy period in most of the region, fire activity in the September-October-November trimester is low in North-SA (see Fig. S3). In this trimester, however, JULES simulates particularly dry conditions in eastern North-SA, resulting in relatively low Gross Primary Production (GPP) (see Fig. S5). This means that dry conditions, rather than carbon availability, might be leading to the overestimations in this period. Since fire activity typically peaks during the drier seasons, seasonal variability in lightning is not expected to have a significant impact on fire activity during this period. For South-SA, INFERNO's CO emissions have lower

average peak magnitudes at the observed inventory peaks (average seasonal cycle of Bias% -79%), with no discernible peak shown in Fig. 3 (e). However, the estimated emissions are higher than the inventories from November to February. Spatially, INFERNO captures the September peak in the northern part of South-SA. However, towards the south, the timing of the emission peak changes rapidly, suggesting a simulated CO emission peak in December and January, when INFERNO shows the largest overestimations of emissions. For the South-SA, both flammability and GPP explain the simulated seasonal cycle in one of the more fire-active zones, the Chaco region (San Martín et al., 2023). Here, although the rainy season coincides with the warmer months (around December to February), the larger dry areas of the Chaco region respond more to wet conditions and vegetation growth than to high temperatures. After this season, late in the colder and drier months (August-September), fire activity and emissions peak as the dry, abundant vegetation ignites. The wetter fraction of the Chaco region additionally peaks in February, as this is more sensitive to temperature and precipitation anomalies (San Martín et al., 2023). Peatlands are not represented in the JULES model, which means that INFERNO does not account for the conditions in the wet Chaco. However, the dry Chaco, which dominates in area, could be more accurately represented. Here, INFERNO's flammability appears to be heavily influenced by temperature and carbon load produced by the increasing GPP (see Fig. S6), so that precipitation does not reduce the likelihood of fires enhanced by the greater carbon availability.

3.1.2 Trends of fire CO emissions in South America

As Fig. 4 shows, the trends in CO emissions between 2004 and 2021 from the inventories are neither consistent nor significant across South America. Spatially, a slight decrease in CO emissions predominantly covers the regions. The decreasing trend in CO emissions is significant across most inventories for some sections of the Arc of Deforestation and the Caatinga ecoregion (eastern part of Brazil), where the trends were around -6% yr^{-1}. GFAS exhibits the strongest trend with a significant decrease of $\sim$2.8% yr^{-1} for the total CO emissions in Mid-SA (see Table 2). Contrary to the inventories, INFERNO shows a weak increasing trend for Mid-SA total emissions (1.6% yr^{-1}), with overall trends overestimating those of the inventories (trend Bias% $\sim$32%). Particularly, the model shows a large increase in emissions in the south of the Amazon forest, which does not agree with the inventories. Similarly, on a finer scale, INFERNO fails to capture the increase in emissions observed near the Caatinga ecoregion, in the large agricultural frontier across the states of Maranhão, Tocantins, Piauí and Bahia in Brazil (Milare et al., 2024; Pope et al., 2020).

In the Mid-SA, both deforestation and dry conditions significantly influence the trend of fire-related CO emissions (Aragão et al., 2018). The relative influence of these and the lack of deforestation representation in INFERNO induce differences in the model's performance over time, affecting the simulated emissions trend. As deforestation in the Amazon gradually declined over the first 10 years of this study (Aragão et al., 2018), the role of drought in facilitating fires became increasingly prominent. For the period from 2004 to 2010 in Mid-SA, INFERNO showed a spatiotemporal Bias% of $\sim$ 30%, indicating higher simulated CO emissions than the inventories (except for GFED5, for which the difference was only -3%). However, from 2011 to 2018, as deforestation ceased, INFERNO estimates rose to $\sim$ 165% above all inventories (see Fig. S7). From 2019 to the end of the study period, both deforestation and drought conditions occurred. In 2019, deforestation in Brazil escalated by approximately 80%, following the relaxation of forest protection regulations (Gatti et al., 2023). At the same time, fire occurrence was further

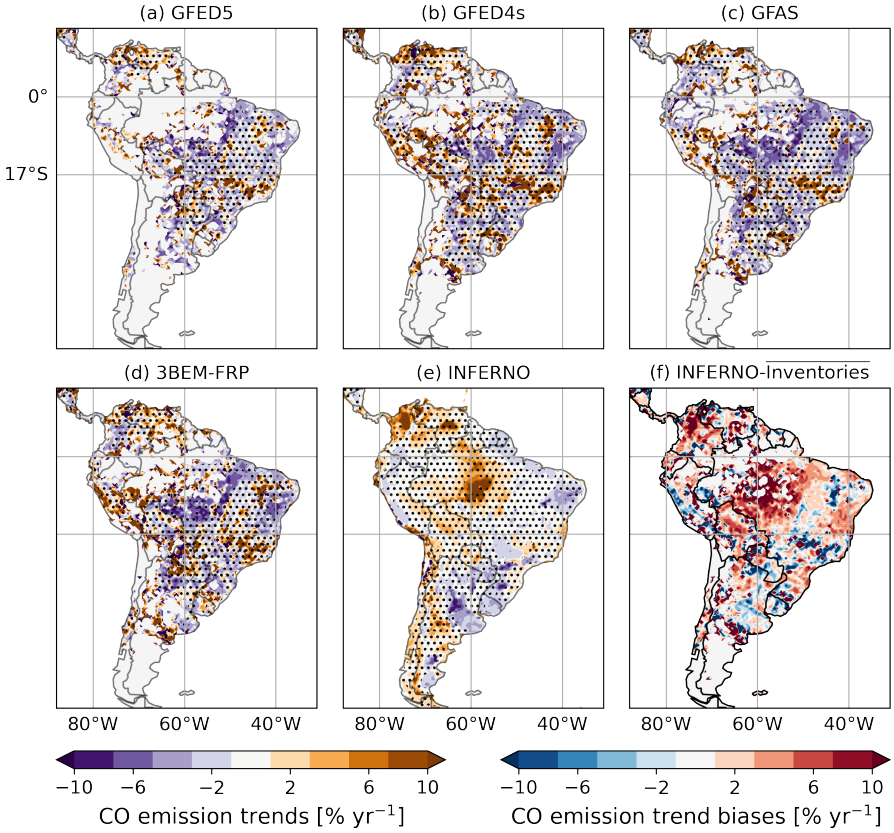

Figure 4. Fire CO emission trend 2004-2021 estimated based on (a) GFED5, (b) GFED4s, (c) GFAS, (d) 3BEM-FRP, and (e) INFERNO. (f) shows the differences between the calculated trend for INFERNO and the average estimates of fire CO emissions. The areas hatched with dots in panels (a-e) indicate when the calculated trend is not significant according to the Mann-Kendall Trend Test; this applies only to areas with nonzero trend.

exacerbated by the extreme drought period in 2019-2022 (Geirinhas et al., 2023). During this period, INFERNO simulated fire emissions in Mid-SA continued to show an overestimation of around 165%. The shift in performance throughout the study period suggests a high sensitivity of the simulations to drought conditions, as flammability has increased over time, together with the overestimations. The trends (see Fig. S8), however, are negative across vast areas because they have been offset by diminishing carbon availability. Furthermore, the changing performance exhibits a potentially misleading offset effect over the overestimations due to the lack of deforestation representation in the model.

In North-SA, as in Table 2, the inventories and INFERNO agree on a weak increase in total annual fire CO emissions, which is only significant for 3BEM-FRP. Despite the weaker annual regional emissions trend, the INFERNO percentage increase in emissions largely covers the northern region. This contrasts with inventory estimates, which suggest a likely decrease in emissions across Colombia's Andean region. Consequently, INFERNO exhibits a broader spatial extent of emission increases,

as illustrated in Fig. 4 (f), and displays a trend bias of 30%. The INFERNO total fire CO emissions for the regions show particularly high magnitudes for 2006-2007 and 2015-2016 (see Fig. S7), which corresponded to weak and strong El Niño events, respectively. The CO emissions from the inventories were also significantly higher during these El Niño events, similar to those for 2019 and 2020. While the INFERNO emissions are similar to the estimates for 2019 and 2020, the emissions magnitudes observed in INFERNO relative to 2006-2007 and 2015-2016 are weaker. The higher emissions in North SA in the latter years of the study period were also associated with the drought conditions and deforestation in the region (Gomes et al., 2021; Amador-Jiménez et al., 2020).

For South-SA, none of the inventories showed a significant trend in CO emissions, and there is no consensus on the direction of a possible trend (see Table 2). From 2019 to 2021, South-SA experienced particularly high fire activity, resulting in CO emissions that were more than 126% higher than the average for the previous five years. INFERNO captured the relative increase, estimating that emissions during this period were approximately 121% higher than those of the preceding five years. According to Geirinhas et al. (2023), the 2019-2021 drought period particularly affected South-SA due to the La Niña phase of the ENSO, combined with the negative phase of the Pacific Decadal Oscillation. The drought conditions were likely exacerbated by the reduction in warm, humid air transported from the Amazon, a situation significantly influenced by deforestation (Marengo et al., 2021) and agricultural expansion in the region (Baumann et al., 2017). In South-SA, increasing deforestation also directly increases fire occurrence, particularly in the last years of the study period (San Martín et al., 2023).

3.2 Sensitivity experiments using INFERNO

The collection of experiments analysing ignition consistently produces lower CO emissions compared to the INFERNO control run (i.e., the model configuration analysed in previous sections). In fact, as Fig. 5 illustrates, these experiments (IT-CST, IT-NAT, and IT-HDI) are the only ones producing significantly lower CO emissions simulations in the Arc of Deforestation region. In general, the differences within the experiment group are subtle, particularly between IT-CST and IT-NAT, which share a constant anthropogenic ignition but have distinct natural ignitions. While anthropogenic ignition remains constant throughout the year for both IT-NAT and IT-CST, natural ignition has a seasonal cycle for IT-NAT. However, both experiments exhibit a similar seasonal cycle, peaking one month before the real peak for Mid-SA and North-SA (see Fig. 6), while maintaining the same erroneous seasonal cycle shape for North-SA and South-SA. These results show that natural ignition makes a negligible contribution to the spatial, seasonality and trends of simulated fire activity in INFERNO over South America (see Fig. 7). The results also indicate a limited constraint on human access to different biome locations, as represented by population density, when simulating ignitions. This is illustrated by IT-CST, which, assuming constant anthropogenic access to the different PFTs, results in lower emissions than in the control run even throughout the Amazon forest. As shown by IT-HDI, the proposed parametrisation of socioeconomic influence strongly reduces emissions, with some benefits (e.g., reducing annual bias in North-SA), but it does not alter the simulated seasonal cycle shape or trends (Fig. S10).

Prescribing different meteorological datasets, ERA5 (control run), 20CRv3 (F-20Cr) and W5E5 (F-W5E5) led to large differences in the CO emissions results, particularly where Tree PFT dominates (see Fig. 5). In particular, the experiment F-20CR, compared with the control run, prescribed lower precipitation for Mid-SA (-13%), reduced soil moisture by 12%,

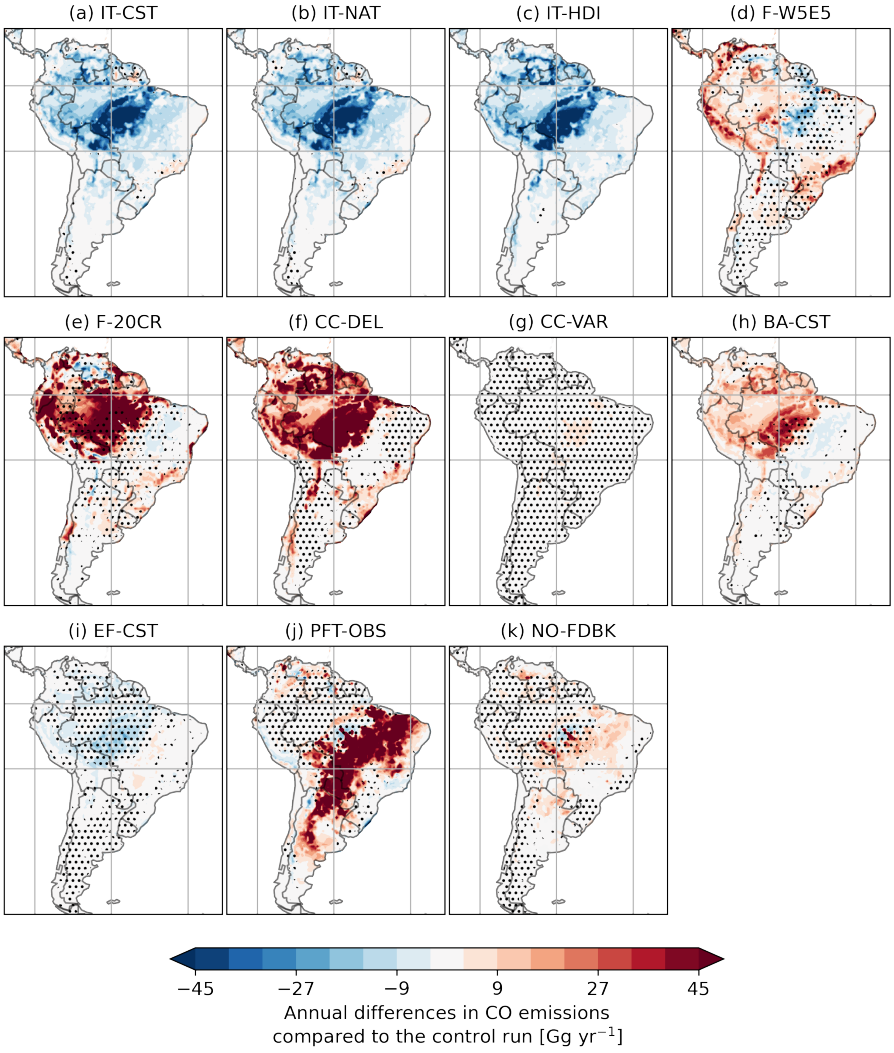

Figure 5. Average annual CO emissions differences between (a-k) each sensitive experiment and the control run model of INFERNO. The control run is the same configuration assessed in Section 3.1. The experiment descriptions are summarised in Table 1. The areas hatched with dots indicate when the simulated and estimated emissions are statistically similar, as determined by the Mann-Whitney test.

445 increased burnt area by 45%, and increased CO emissions by 118%, based on the Bias%. Meanwhile, for the same region, F-W5E5 prescribed (-7%) less precipitation, which consistently reduced soil moisture by 7%, increased burnt area by 17%, and increased emissions by 11%, compared to the control run. Both experiments reduced the available carbon by 7%. From this, and given that soil moisture and carbon load are the main factors describing the seasonal cycle in INFERNO, we found a dominant effect of meteorological conditions. Remarkably, in North-SA, the distinct meteorological conditions in F-20Cr

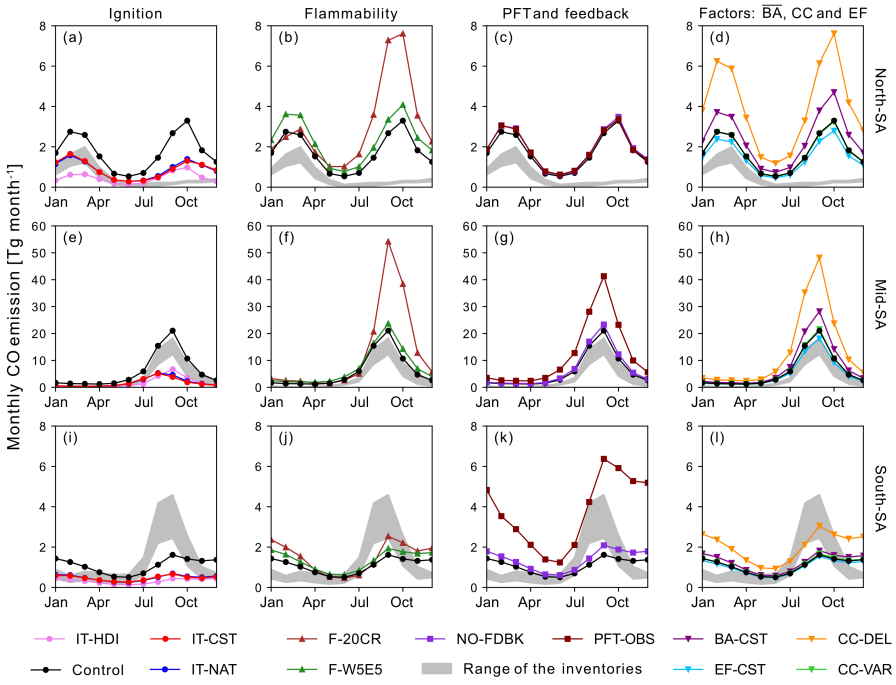

Figure 6. CO emissions seasonal cycle modelled by the different INFERNO experiments and control run in (a-d) North-SA, (e-h) Mid-SA and (i-l) South-SA. The description of the experiment can be found in Section 2.4.

resulted in higher magnitudes of CO emissions at the wrong annual peak of emissions, as Tree PFTs are particularly influenced by drier conditions.

The effect of meteorological conditions was also observed for CC-DEL, where unconstrained soil moisture was used to simulate burnt carbon. The experiment results in increased CO emissions in the south of the Amazon forest and towards the north. In Tree PFT dominant areas, eliminating the constraints (i.e., $CC_{max,wood}$) permits the model to burn the whole wood carbon in the drier season, while the control experiment burnt up to 40%. This is despite the fact that the minimum leaf carbon threshold was reduced to 0.0 from 0.2, meaning a reduction in emissions from this carbon pool in CC-DEL. The experiment results in a small change in CO emissions for East Mid-SA and South-SA, where less Tree PFT is modelled. This result supports the consistent finding that Tree PFTs are more sensitive to dry conditions than other PFTs. The experiment also demonstrates that soil moisture plays a crucial role in capturing the effects of dryness. However, while the experiment reveals the impact of soil moisture on emissions, it does not reflect its influence on the burnt area, which is the same for both CC-DEL and the control run. It should be noted that changes in CC factors over wood and leaf do not directly affect the carbon loss output to JULES. This is because other combustion completeness parameters are used for outputting the carbon lost in JULES (Burton et al., 2019), and we did not change them. As a consequence, the calculated trend differs little from that in the control run.

While the CC-DEL experiment highlights how strongly $CC_{max,wood}$ can shape soil moisture effect, CC-VAR demonstrates that discrete changes and adding PFT dependence in the factors lead to negligible changes (see Fig. 7). The results here

might be due to $CC_{max,wood}$ not being adjusted for the tree PFTs, which use the same values as the control run. Based on the literature, we set lower $CC_{min,leaf}$ for tree PFT and higher $CC_{max,wood}$ for grasses and pastures. Nonetheless, as Fig. 5 shows, the CO emissions simulated from CC-VAR are not significantly different from those simulated by the control run, which uses constant CC values regardless of PFT. The results suggest that from the CC factors, the $CC_{max,wood}$ tends to be the main factor constraining soil moisture in the simulation of burnt carbon (see Equation 6).

As noted, Tree PFTs, particularly Broadleaf Deciduous Trees and Tropical Broadleaf Evergreen Trees, play a key role in controlling how changes in model factors (e.g., CC, $\overline{BA}$) affect simulations over South America. Building on this, BA-CST and EF-CST experiments with average constant for $\overline{BA}$ and EF_{CO} resulted in increased and decreased emissions, respectively, compared to the control run (see Fig. 7). These outcomes are due to the relatively low $\overline{BA}$ and high EF_{CO} characteristic of Tree PFTs. Notably, the impact of BA-CST was especially pronounced in the southern Amazon and northern South America. Overall, BA-CST differs more from the control run than EF-CST, with greater spatial variation as well as differences in the amplitude and trend of the seasonal cycle.

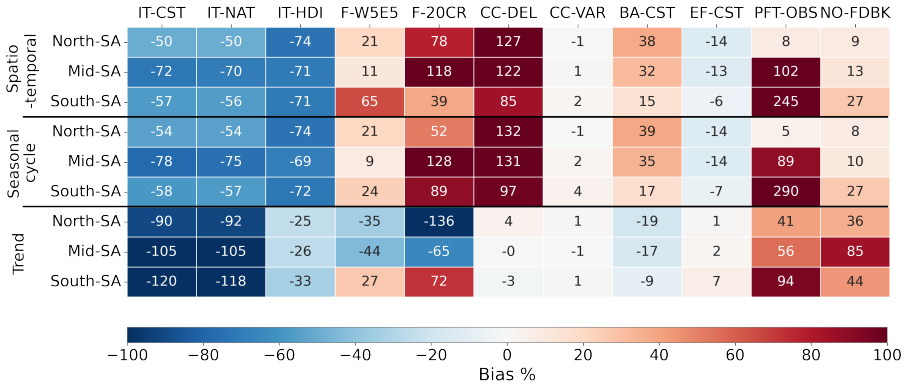

Figure 7. CO emissions spatiotemporal, seasonal cycle and trend percentage mean bias (Bias%) for the sensitive experiments based on the control run of INFERNO. The Bias% are shown independently for the study regions in South America. The trends of fire CO emissions calculated for the sensitivity experiments are shown in Fig. S10.

Changing the PFT (i.e., PFT-OBS) results in a few changes in the southern Amazon forest, even when the Tropical Broadleaf Evergreen Trees greatly dominate over the simulated Broadleaf Deciduous Trees (see Fig. S2). As Fig. 5 shows, the main difference between this experiment and the control run is seen in the east of Mid-SA and in South-SA, where higher emissions are observed in regions with dominant grasses and pastures. In this region, the PFT-OBS tends to exhibit a higher tree fraction, greater wood carbon availability, and consequently higher CO emissions. Using observations of vegetation to represent PFTs did not improve the simulated emissions nor the seasonal cycle representation in Mid-SA or South-SA (see Fig. S9). Still, they did increase CO emissions in South-SA to the estimated range from the inventories during the peak of emissions, while in Mid-SA the emissions were further overestimated (see Fig. 6).

Although all experiments lack feedback from the atmosphere, as this is a land-only model, the results from the NO-FDBK experiment illustrates the proportional error that the omission of feedback to land can introduce into the fire model. According to the experiment, this omission results in significant increases in the spatiotemporal magnitudes and seasonal cycle amplitudes of the simulated CO emissions (Bias% $\sim$ 15%). However, as expected, it does have a more substantial influence on the simulated trends, where differences against the control run have a Bias% of 85% in Mid-SA. The No-FDBK experiment results in spatiotemporal CO emissions that are approximately 94% higher than the inventory estimates for Mid-SA, which is 22% higher than the Bias% observed in the control run ($\sim$72%) compared to the inventories (see Table 2).

3.3 Explaining INFERNO CO Emission Biases Using Machine Learning

Across the five-fold cross-validation iterations, the XGBoost model achieved an average R^2 of 0.67. The mean RMSE was 6.6 Gg yr^{-1}, corresponding to approximately the 75th percentile of the absolute magnitude of the target variable (CO emission biases). The MAE averaged 2.5 Gg yr^{-1}, close to the median absolute bias. Overall, the XGBoost model explains 67% of the variability in the target variable; however, the prediction errors remain comparable to or greater than the median of INFERNO CO emission absolute biases. Notably, the machine learning model struggles to capture negative biases (see Fig. S12). However, the model is particularly well-suited to explaining the overestimation of CO emissions in Mid-SA, where most fire activity and the INFERNO large absolute biases are concentrated.

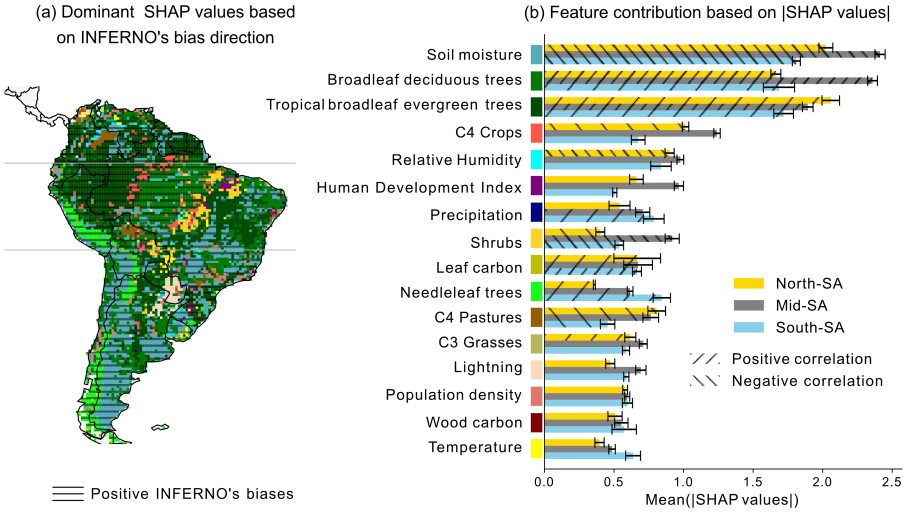

Figure 8. (a) Gridded dominant feature contribution of the XGBoost model according to the bias direction and (b) feature contribution to the XGBoost-predicted biases using absolute SHAP values. The horizontal line hatched area in (a) describes where INFERNO CO emissions biases are, on average, positive. The forward and back diagonal hatched bars in (b) indicate respectively when the magnitude of the variable correlates positively (R > 0.5) or negatively (R < -0.5) with their contribution to the modelled CO emission biases. The respective hatch is more frequent when the correlation is stronger (|R| > 0.7). Notice that this figure does not include all XGBoost features, as the three with the lowest SHAP values were omitted.

Figure 8 illustrates the feature contributions at two levels: gridded (a) and regional (b). Since SHAP values can be both positive and negative, we used the absolute SHAP values for the subregional assessment. We focused on the larger positive or negative SHAP values to characterise the dominant contributions associated with the bias direction in the gridded map. According to the SHAP values, soil moisture and the tree PFT Broadleaf Deciduous Trees and Tropical Broadleaf Evergreen Trees particularly stand out in driving INFERNO biases. This aligns with the particular sensitivity that INFERNO showed regarding these variable changes in Section 2.4. Despite the low correlation between soil moisture and the biases (R = 0.18, see Fig. S11), soil moisture is the top variable to explain and then address the spatiotemporal biases of INFERNO in South America. As Fig. 8 shows, the SHAP values of soil moisture negatively correlate with soil moisture magnitudes in the three regions (R $\sim$ -0.8), showing that low values of soil moisture tend to explain high positive biases of CO emissions, while negative or low biases are present when there are wetter conditions.

The fractions of Broadleaf Deciduous Trees and Tropical Broadleaf Evergreen Trees show a strong positive correlation of their contribution to predicting CO emission biases. Higher proportions of these PFTs are associated with positive biases, particularly in North-SA and Mid-SA. The results also suggest that low values of the Tree PFTs contribute to modelling the lower and/or negative bias of INFERNO CO emissions. Spatially, it is clear that Broadleaf Deciduous Trees and Tropical Broadleaf Evergreen Trees are the dominant feature of importance where INFERNO overestimates CO emissions in the Amazon rainforest (see Fig. 8.b). However, the more frequent contribution of the variable toward negative biases in South-SA is probably related to the fact that tree fractions are underestimated in this region. Particularly, in the Chaco ecoregion, the underestimation is evident when comparing TRIFFID and the ESA land-cover-based PFTs (see Fig. S2). In 2019, the tree cover fraction in Chaco was over 30%; however, Scrublands dominated in the Dry Chaco (38.2%) (San Martín et al., 2023). However, TRIFFID modelled C4 Grasses, C4 Pastures, and bare soil are dominant PFTs with 88% cover in the Chaco region; none of the Tree PFTs had an average fraction over 2%. This aligns well with the results of the experiment prescribing PFT, PFT-OBS. PFT-OBS, which had higher CO emissions than the control run in areas of previous underestimation.

The crop fraction, C4 Crops, ranks fourth in its contribution to explaining CO emission biases. C4 Crops SHAP values negatively correlate with the PFT fractions in North-SA (R=-0.52), particularly describing positive biases when the fraction of this PFT is low. Surprisingly, the fraction dominates inside the Amazon forest near the Amazon River. The C4 Crops contribution is also dominant around the Arc of Deforestation, along with Shrub fractions, which correlates negatively with its contribution to biases (R=-0.70). Therefore, the high fraction seems to be related to negative biases.

Finally, although the INFERNO configuration in this study did not include HDI, this feature shows potential to address INFERNO CO emission biases. However, its contribution to address them is not linear as it weakly correlates with HDI magnitudes. In North-SA, the correlation is 0.48, indicating that higher HDI is associated with positive biases. This aligns with the results from Teixeira et al. (2021), which suggested that countries with high living standards may more easily suppress fires, resulting in lower CO emissions than simulations that do not include the HDI.

4 Discussion

4.1 INFERNO performance and main factors explaining biases

The results of this study were consistent in showing that soil moisture, particularly low magnitudes, and Tree PFTs in South America are the top drivers of biases in INFERNO. The few inputs used by INFERNO to represent anthropogenic influence on fire ranked after these meteorological and vegetation conditions; however, including more socioeconomic factors could help explain the remaining 33% of the bias in the XGBoost model.

The XGBoost model identified soil moisture as the primary variable explaining the biases observed in INFERNO, while relative humidity also emerged as a significant factor related to meteorological conditions. The lack of global, long-term soil moisture datasets has prevented the assessment of the direct effect of soil moisture on the performance of fire models (Hantson et al., 2020). Nonetheless, other variables that describe drought conditions have been assessed. According to Forkel et al. (2019)'s evaluation, for INFERNO, maximum temperature contributes the most to the simulated burnt area, even more than for other models. However, wet conditions, represented by the number of days with significant precipitation, had little influence on burnt area (Forkel et al., 2019). Although reported with different variables, the role of dry conditions in INFERNO, identified by Forkel et al. (2019), supports the observed sensitivity to soil moisture, as this was also particularly evident in INFERNO simulations under dry conditions. Still, both studies differ in evaluation targets, the independent variables selected, and the variations in temporal and spatial resolution. Furthermore, burnt areas may be less sensitive to soil moisture than CO emissions, as evidenced by experiments that varied meteorological conditions. This observation is consistent with the results reported by Mathison et al. (2023), where INFERNO produced stable results for the burnt area across various meteorological datasets.

Our evaluation consistently supports that INFERNO-simulated CO emissions were too sensitive to drier conditions, particularly in Broadleaf Deciduous Trees (see Fig. S13). In fact, Teckentrup et al. (2019) shows that increasing probability of fires driven by soil moisture begins to manifest in wetter conditions for INFERNO than for other models. In general, most overestimations relative to the inventories were in areas where modelled Broadleaf Deciduous Trees and Tropical Broadleaf Evergreen Trees dominate. The control of the Tree PFTs is particularly clear around the Arc of Deforestation in Mid-SA, where the relative fraction of these two tree PFTs appears to shape this main source of CO emissions in South America. In North-SA, with lower absolute emissions, the sensitivity of Tree-PFT to drought conditions underpinned the incorrect representation of the seasonal cycle. There, fire emissions from the Tree PFTs were incorrectly simulated with similar magnitudes to the fire-prone Llanos ecoregion emissions, where pasture is the dominant modelled PFT. Furthermore, the role of drought conditions in Tree PFTs was evident in the increasing biases over time, consistent with the growing influence of drought events. Finally, the large differences in simulated CO emissions resulting from different meteorological datasets used as inputs to JULES indicate that the response to drought conditions in Tree PFTs-dominated areas outweighs the influence of carbon availability, particularly in shaping the seasonal cycle of emissions. Compared with other models, the INFERNO fuel load index reaches its maximum much more rapidly in response to fuel density (Teckentrup et al., 2019), which is why, with high carbon availability, changes in fuel density may lead to muted differences.

Tree PFTs as top factors to describe CO emissions biases were associated with both overestimations and underestimations, according to the XGBoost model. INFERNO simulations underestimate CO emissions in key South America ecoregions: Cerrado, Llanos and Chaco. In JULES, these ecoregions tend to be dominated by modelled C4 Pastures and Grasses (see Fig. S13). According to the machine learning results, the Broadleaf Deciduous Trees fraction is the main factor explaining the underestimation of emissions in these ecoregions, given its low abundance. Indeed, for the Chaco region, we observed likely underestimation of the Tree PFTs fraction compared to observation-based PFTs and the literature (Harper et al., 2023; San Martín et al., 2023). In our experiments, using observation-based PFTs increases emissions estimates in the three ecoregions, but less so in the Llanos. Consistently, it has been suggested that INFERNO biases might be enhanced by disproportionately reducing the Tree fraction in savannas (Mathison et al., 2023), to which the model simulations seems highly sensitive (Teixeira et al., 2021; Mathison et al., 2023).

In South-SA, a significant portion of the trees in the dominated pasture and grass areas may be consumed due to the incorrectly simulated two-peak fire activity. In general, the seasonal cycle of emissions in the southern extratropics varies significantly, and fire models often struggle to accurately reflect this variability (Hantson et al., 2020). As in INFERNO, simulations frequently emphasise the global peak in December-January (Hantson et al., 2020). Our findings indicate that the simulated seasonal cycle of CO emissions by INFERNO closely follows the rise in GPP and flammability during December-January, a period marked by high temperatures and rainfall. As shown by Teckentrup et al. (2019), the INFERNO fuel load index, which is used in the flammability calculation, is highly sensitive to minor changes in fuel density when the overall fuel amount is small. Therefore, even during the rainy season, there may be hot days without rain, during which the relative humidity is sufficiently low to enable flammability to peak according to the fuel load index.

Ranked fourth in contributing to bias prediction in the XGBoost model, the low fraction of C4 crops explains the positive CO emissions bias. As this feature particularly dominates in explaining biases in the Amazon, the feature is likely representing the lack of anthropogenic activities. In INFERNO, the anthropogenic ignition representation does not seem well-bounded by population density, as even constant ignitions result in lower CO emissions in the centre of the Amazon forest, where almost no fires occur. The representation of anthropogenic activities and threats, including crop and deforestation, is a factor largely missing in the global fire modelling community (Hantson et al., 2020). In general, there is substantial disagreement over the response of modelled fire activity to socioeconomic factors (Forkel et al., 2019). In the XGBoost model, HDI also ranked high, which helps explain the underestimation of CO emissions. In the machine learning model, the low values of the index push the bias toward negative biases. The findings aligns with the idea that countries with, in this case, low living standards may face more difficulties in suppressing fires, resulting in higher burnt area and CO emissions (Teixeira et al., 2021).

4.2 Implications for future development

Soil moisture is the top factor limiting fire activity in tropical forests (Kelley et al., 2019). This variable is widely used in fire models, as in INFERNO, to describe fuel moisture (Rabin et al., 2017). However, using soil moisture to represent fuel moisture without a PFT-dependent factor might lead to incorrect representation, as fuel moisture, particularly in live plants, depends on soil conditions and plant physiology (Forkel et al., 2023). This incorrect representation is pronounced for forest land covers,

where the correlation between soil moisture and live fuel moisture content is low, with a long lag time for the best correlation (Vinodkumar et al., 2021). For INFERNO, the combustion completeness factor, particularly $CC_{max,wood}$, varying across PFTs, could be utilised to diminish the effect of soil moisture on CO emissions. As shown in the study, this particularly constrains the soil moisture effect in the simulated burnt carbon. Similarly, although the burnt area's over response to soil moisture might be weaker, targeting fuel moisture representation in flammability can help capture better the seasonal cycle variability of fire activity. Multiple variables to describe the fuel moisture content on fire danger can be used instead of or in synergy with soil moisture, such as fire danger indexes (e.g. the Nesterov index) (Drüke et al., 2019; Rabin et al., 2017). For South America, Drüke et al. (2019) show improved representation of the burnt area using a vapour-pressure-deficit-based fire danger index in flammability calculation. The Fire Weather Index and Nesterov Fire Index are readily testable, as they are already calculated along with burnt area and emissions by INFERNO (Mangeon et al., 2016).

Socioeconomic factors have, overall, demonstrated diverse influences on fire activity across different parts of the world, making it very difficult to capture in a fire model (Forkel et al., 2019). Including deforestation representation and crop influence has shown little improvement (Hantson et al., 2020; Gallup et al., 2024), particularly in the accuracy of fine-scale representation, which remains unattainable at this stage (Gallup et al., 2024). However, it has been observed that including or excluding crops in fire models can yield different trends in burnt area and emissions (Li et al., 2019). In this study, Crops were particularly highlighted as a possible variable to bound the extent of biases due to anthropogenic factors. However, the XGBoost model's missing 33% of bias representation indicates that a fairly large portion of the bias is not explained by the current INFERNO inputs. Therefore, bias in Crop representation could be reduced by incorporating additional information beyond its fraction. In a fire model, crop representation needs to include the agriculture management cycle (Li et al., 2013), the influence of socioeconomic factors on management practices (Li et al., 2013), agricultural expansion, and landscape fragmentation (Silva-Junior et al., 2022), among others. Crop representation would also need to include the agricultural role in fire suppression (Haas et al., 2022). To include a representation of deforestation in fire models, parameters such as the deforestation rate, human accessibility represented by distance to roads and rivers, could be explored (Haas et al., 2022; dos Reis et al., 2021).

In regions such as South America, individually representing deforestation in INFERNO can increase simulated fire emissions and, in turn, exacerbate biases that hinder their potential improvement. At the same time, having a more accurate response to soil moisture would reduce emissions, possibly below estimates, making the lack of deforestation representation more visible. Both developments individually would yield no obvious benefit compared to emissions inventories, but would improve the model's ability to represent fire-relevant processes. We recommend evaluating the benefits of this development, weighing the interannual variability of the simulated factors and derived consequences on the model. Additionally, pursuing synergistic development could provide added advantages.

4.3 Future work

This study has a number of limitations, which offer opportunities for further research and improvement. For the sensitivity analysis, we employed a one-at-a-time approach, which is the reason why only a few experiments were run across the full range of input variability. Therefore, we see significant benefits in utilising methods such as the perturbed ensemble member

approach. We recommend paying special attention to the interactions between soil moisture and PFT. Furthermore, in this study, we used similar weighted-average estimates to calculate the biases modelled by the XGBoost model. For this, employing a weighted average based on inventory performance would allow for a more accurate benchmark. Alternatively, to better account for the uncertainty introduced by multiple inventories, an approach could involve running multiple machine learning models to target the different biases present across them. Finally, while we aim to identify pathways for improvement using the current inputs to INFERNO, incorporating additional variables into the machine learning model could help address further, even fine-scale, biases.

Code and data availability. The JULES-ES control configuration (based on JULES version 7.5) is stored at [https://code.metoffice.gov.uk/trac/roses-u/browser/d/l/3/2/3/trunk, last access:11 March 2025]. JULES and associated configurations are freely available for non-commercial research use, as set out in the JULES user terms and conditions [http://jules-lsm.github.io/access_req/JULES_Licence.pdf, last access: 10 November 2025]. For a comprehensive guide to accessing, installing, and running the configurations, we direct the reader to Appendix A in Wiltshire et al. (2020). Note that to view and use the JULES-ES source code, access will be required via the Met Office Science Repository Service [https://code.metoffice.gov.uk/trac/home, last access: 10 November 2025], and is available to those who have signed the JULES user agreement. The easiest way to access the repository is to complete the online form to register at [http://jules-lsm.github.io/access_req/JULES_access.html, last access: 10 November 2025].

The fire CO emission are downloaded from the inventories GFEDvn5 at [https://surfdrive.surf.nl/files/index.php/s/VPMEYinPeHtWVxn, last access: 18 November 2025], GFEDvn4s [https://daac.ornl.gov/VEGETATION/guides/fire_emissions_v4_R1.html, last access: 20 October 2025] (van der Werf et al., 2017), GFASvn1.2 [https://ads.atmosphere.copernicus.eu/datasets/cams-global-fire-emissions-gfas?tab=overview, last access: 18 November 2025] (Kaiser et al., 2012). The 3BEM-FRP dataset was provided directly by (Pereira et al., 2022). The HDI datasets were downloaded on a national scale [https://datadryad.org/dataset/doi:10.5061/dryad.dk1j0, last access: 18 November 2025] and on a subnational scale from [https://globaldatalab.org/shdi/, last access: 18 November 2025]. Some assessments were done using the deforestation front for 2020 provided at [https://globil.panda.org/datasets/panda::deforestation-fronts-2020-1/about, last access: 18 November 2025] and the ecoregion for 2017 provided at [https://ecoregions.appspot.com/, last access: 18 November 2025]. The model inputs are provided by ISIMIP3a at [https://protocol.isimip.org/#/ISIMIP3a/fire, last access: 18 November 2025].The fire CO emissions simulated by the experiments included in this study, together with the JULES outputs used in the machine learning model and the simulated burn area and flammability, are on Zenodo at [https://doi.org/10.5281/zenodo.18337852, Velásquez-García et al. (2026)].

Author contributions. All the authors participated in reviewing and editing this manuscript. Additionally, MPV: conceptualisation; data curation; formal analysis; investigation; methodology; software; visualisation; writing (original draft). RJP: conceptualisation; investigation; methodology; supervision; project administration. STT: conceptualisation; investigation; methodology; supervision; project administration. CD: methodology. DPM: resources. GM: resources. MPC: project administration.

Competing interests. The contact author has declared that none of the authors has any competing interests.

Acknowledgements. We thank the NCAS Computational Modelling Services Helpdesk for the software support regarding JULES-INFERNO. The authors also thank Camilla Mathison, Eleanor Burke, and Rich Ellis for their help in setting up the suite. This work was funded by

the UK Natural Environment Research Council (NERC), which provided funding for the National Centre for Earth Observation (NCEO; grant no. NE/R016518/1, NE/X019071/1 and NE/R016518/1) and the NERC Panorama Doctoral Training Partnership (DTP; grant no. NE/S007458/1). The contributions of Steven Turnock were funded by the Met Office Climate Science for Service Partnership (CSSP) China project under the International Science Partnerships Fund (ISPF). São Paulo Research Foundation (FAPESP; grants 2025/07124-4, 2025/28244-8) funded the contributions from Guilherme Mataveli.

References

Akagi, S. K., Yokelson, R. J., Wiedinmyer, C., Alvarado, M. J., Reid, J. S., Karl, T., Crounse, J. D., and Wennberg, P. O.: Emission factors for open and domestic biomass burning for use in atmospheric models, Atmospheric Chemistry and Physics, 11, 4039–4072, https://doi.org/10.5194/acp-11-4039-2011, 2011.

Amador-Jiménez, M., Millner, N., Palmer, C., Pennington, R. T., and Sileci, L.: The Unintended Impact of Colombia's Covid-19 Lockdown on Forest Fires, Environmental and Resource Economics, 76, 1081–1105, https://doi.org/10.1007/s10640-020-00501-5, 2020.

Andreae, M. O. and Merlet, P.: Emission of trace gases and aerosols from biomass burning, Global Biogeochemical Cycles, 15, 955–966, https://doi.org/10.1029/2000GB001382, 2001.

Aragão, L. E. O. C., Anderson, L. O., Fonseca, M. G., Rosan, T. M., Vedovato, L. B., Wagner, F. H., Silva, C. V. J., Junior, C. H. L. S., Arai, E., Aguiar, A. P., Barlow, J., Berenguer, E., Deeter, M. N., Domingues, L. G., Gatti, L., Gloor, M., Malhi, Y., Marengo, J. A., Miller, J. B., Phillips, O. L., and Saatchi, S.: 21st Century drought-related fires counteract the decline of Amazon deforestation carbon emissions, Nature Communications, 9, 536, https://doi.org/10.1038/s41467-017-02771-y, 2018.

Baumann, M., Gasparri, I., Piquer-Rodríguez, M., Gavier Pizarro, G., Griffiths, P., Hostert, P., and Kuemmerle, T.: Carbon emissions from agricultural expansion and intensification in the Chaco, Global Change Biology, 23, 1902–1916, https://doi.org/10.1111/gcb.13521, 2017.

Bauters, M., Drake, T. W., Verbeeck, H., Bodé, S., Hervé-Fernández, P., Zito, P., Podgorski, D. C., Boyemba, F., Makelele, I., Ntaboba, L. C., Spencer, R. G. M., and Boeckx, P.: High fire-derived nitrogen deposition on central African forests, Proceedings of the National Academy of Sciences, 115, 549–554, https://doi.org/10.1073/pnas.1714597115, 2018.

Beckett, H., Staver, A. C., Charles-Dominique, T., and Bond, W. J.: Pathways of savannization in a mesic African savanna–forest mosaic following an extreme fire, Journal of Ecology, 110, 902–915, https://doi.org/10.1111/1365-2745.13851, 2022.

Burton, C., Betts, R., Cardoso, M., Feldpausch, T. R., Harper, A., Jones, C. D., Kelley, D. I., Robertson, E., and Wiltshire, A.: Representation of fire, land-use change and vegetation dynamics in the Joint UK Land Environment Simulator vn4.9 (JULES), Geoscientific Model Development, 12, 179–193, https://doi.org/10.5194/gmd-12-179-2019, 2019.

Burton, C., Betts, R. A., Jones, C. D., Feldpausch, T. R., Cardoso, M., and Anderson, L. O.: El Niño driven changes in global fire 2015/16, Frontiers in Earth Science, 8, 199, https://doi.org/10.3389/feart.2020.00199, 2020.

Burton, C., Kelley, D. I., Jones, C. D., Betts, R. A., Cardoso, M., and Anderson, L.: South American fires and their impacts on ecosystems increase with continued emissions, Climate Resilience and Sustainability, 1, e8, https://doi.org/10.1002/cli2.8, 2022.

Burton, C., Lampe, S., Kelley, D. I., Thiery, W., Hantson, S., Christidis, N., Gudmundsson, L., Forrest, M., Burke, E., Chang, J., Huang, H., Ito, A., Kou-Giesbrecht, S., Lasslop, G., Li, W., Nieradzik, L., Li, F., Chen, Y., Randerson, J., Reyer, C. P. O., and Mengel, M.: Global burned area increasingly explained by climate change, Nature Climate Change, 14, 1186–1192, https://doi.org/10.1038/s41558-024-02140-w, 2024.

Chen, T., He, T., Benesty, M., Khotilovich, V., Tang, Y., Cho, H., Chen, K., Mitchell, R., Cano, I., Zhou, T., Li, M., Xie, J., Lin, M., Geng, Y., Li, Y., Yuan, J., and Cortes, D.: XGBoost Parameters, https://xgboost.readthedocs.io/en/latest/parameter.html, 2025.

Chen, Y., Hall, J., van Wees, D., Andela, N., Hantson, S., Giglio, L., van der Werf, G. R., Morton, D. C., and Randerson, J. T.: Multi-decadal trends and variability in burned area from the fifth version of the Global Fire Emissions Database (GFED5), Earth System Science Data, 15, 5227–5259, https://doi.org/10.5194/essd-15-5227-2023, 2023.

Cummings, A. R., Kennady, B. J., and Adeuga, A. M.: Fire Regions of a Northern Amazonian Landscape Relative to Indigenous Peoples' Lands, Remote Sensing, 17, https://doi.org/10.3390/rs17193386, 2025.

Dinerstein, E., Olson, D., Joshi, A., Vynne, C., Burgess, N. D., Wikramanayake, E., Hahn, N., Palminteri, S., Hedao, P., Noss, R., Hansen, M., Locke, H., Ellis, E. C., Jones, B., Barber, C. V., Hayes, R., Kormos, C., Martin, V., Crist, E., Sechrest, W., Price, L., Baillie, J. E. M., Weeden, D., Suckling, K., Davis, C., Sizer, N., Moore, R., Thau, D., Birch, T., Potapov, P., Turubanova, S., Tyukavina, A., de Souza, N., Pintea, L., Brito, J. C., Llewellyn, O. A., Miller, A. G., Patzelt, A., Ghazanfar, S. A., Timberlake, J., Klöser, H., Shennan-Farpón, Y., Kindt, R., Lillesø, J.-P. B., van Breugel, P., Graudal, L., Voge, M., Al-Shammari, K. F., and Saleem, M.: An Ecoregion-Based Approach to Protecting Half the Terrestrial Realm, BioScience, 67, 534–545, https://doi.org/10.1093/biosci/bix014, 2017.

dos Reis, M., de Alencastro Graça, P. M. L., Yanai, A. M., Ramos, C. J. P., and Fearnside, P. M.: Forest fires and deforestation in the central Amazon: Effects of landscape and climate on spatial and temporal dynamics, Journal of Environmental Management, 288, 112 310, https://doi.org/10.1016/j.jenvman.2021.112310, 2021.

Drüke, M., Forkel, M., von Bloh, W., Sakschewski, B., Cardoso, M., Bustamante, M., Kurths, J., and Thonicke, K.: Improving the LPJmL4-SPITFIRE vegetation–fire model for South America using satellite data, Geoscientific Model Development, 12, 5029–5054, https://doi.org/10.5194/gmd-12-5029-2019, 2019.

Forkel, M., Andela, N., Harrison, S. P., Lasslop, G., van Marle, M., Chuvieco, E., Dorigo, W., Forrest, M., Hantson, S., Heil, A., Li, F., Melton, J., Sitch, S., Yue, C., and Arneth, A.: Emergent relationships with respect to burned area in global satellite observations and fire-enabled vegetation models, Biogeosciences, 16, 57–76, https://doi.org/10.5194/bg-16-57-2019, 2019.

Forkel, M., Schmidt, L., Zotta, R.-M., Dorigo, W., and Yebra, M.: Estimating leaf moisture content at global scale from passive microwave satellite observations of vegetation optical depth, Hydrology and Earth System Sciences, 27, 39–68, https://doi.org/10.5194/hess-27-39-2023, 2023.

Frieler, K., Volkholz, J., Lange, S., Schewe, J., Mengel, M., del Rocío Rivas López, M., Otto, C., Reyer, C. P. O., Karger, D. N., Malle, J. T., Treu, S., Menz, C., Blanchard, J. L., Harrison, C. S., Petrik, C. M., Eddy, T. D., Ortega-Cisneros, K., Novaglio, C., Rousseau, Y., Watson, R. A., Stock, C., Liu, X., Heneghan, R., Tittensor, D., Maury, O., Büchner, M., Vogt, T., Wang, T., Sun, F., Sauer, I. J., Koch, J., Vanderkelen, I., Jägermeyr, J., Müller, C., Rabin, S., Klar, J., Vega del Valle, I. D., Lasslop, G., Chadburn, S., Burke, E., Gallego-Sala, A., Smith, N., Chang, J., Hantson, S., Burton, C., Gädeke, A., Li, F., Gosling, S. N., Müller Schmied, H., Hattermann, F., Wang, J., Yao, F., Hickler, T., Marcé, R., Pierson, D., Thiery, W., Mercado-Bettín, D., Ladwig, R., Ayala-Zamora, A. I., Forrest, M., and Bechtold, M.: Scenario setup and forcing data for impact model evaluation and impact attribution within the third round of the Inter-Sectoral Impact Model Intercomparison Project (ISIMIP3a), Geoscientific Model Development, 17, 1–51, https://doi.org/10.5194/gmd-17-1-2024, 2024.

Gallup, S. M., Ford, B., Naus, S., Gallup, J. L., and Pierce, J. R.: Equations to Predict Carbon Monoxide Emissions from Amazon Rainforest Fires, Fire, 7, https://doi.org/10.3390/fire7120477, 2024.

Gatti, L. V., Basso, L. S., Miller, J. B., Gloor, M., Domingues, L. G., Cassol, H. L. G., Tejada, G., Aragão, L. E. O. C., Nobre, C., Peters, W., Marani, L., Arai, E., Sanches, A. H., Corrêa, S. M., Anderson, L., Randow, C. V., Correia, C. S. C., Crispim, S. P., and Neves, R. A. L.: Amazonia as a carbon source linked to deforestation and climate change, Nature, 595, 388–393, https://doi.org/10.1038/s41586-021-03629-6, 2021.

Gatti, L. V., Cunha, C. L., Marani, L., Cassol, H. L., Messias, C. G., Arai, E., Denning, A. S., Soler, L. S., Almeida, C., Setzer, A., et al.: Increased Amazon carbon emissions mainly from decline in law enforcement, Nature, 621, 318–323, https://doi.org/10.1038/s41586-023-06390-0, 2023.

Geirinhas, J. L., Russo, A. C., Libonati, R., Miralles, D. G., Ramos, A. M., Gimeno, L., and Trigo, R. M.: Combined large-scale tropical and subtropical forcing on the severe 2019–2022 drought in South America, npj Climate and Atmospheric Science, 6, 185, https://doi.org/10.1038/s41612-023-00510-3, 2023.

Gomes, M. S., de Albuquerque Cavalcanti, I. F., and Müller, G. V.: 2019/2020 drought impacts on South America and atmospheric and oceanic influences, Weather and Climate Extremes, 34, 100 404, https://doi.org/10.1016/j.wace.2021.100404, 2021.

Haas, O., Prentice, I. C., and Harrison, S. P.: Global environmental controls on wildfire burnt area, size, and intensity, Environmental Research Letters, 17, 065 004, https://doi.org/10.1088/1748-9326/ac6a69, 2022.

Hamilton, D. S., Perron, M. M., Bond, T. C., Bowie, A. R., Buchholz, R. R., Guieu, C., Ito, A., Maenhaut, W., Myriokefalitakis, S., Olgun, N., Rathod, S. D., Schepanski, K., Tagliabue, A., Wagner, R., and Mahowald, N. M.: Earth, Wind, Fire, and Pollution: Aerosol Nutrient Sources and Impacts on Ocean Biogeochemistry, Annual Review of Marine Science, 14, 303–330, https://doi.org/10.1146/annurev-marine-031921-013612, 2022.

Hanan, E. J., Kennedy, M. C., Ren, J., Johnson, M. C., and Smith, A. M. S.: Missing Climate Feedbacks in Fire Models: Limitations and Uncertainties in Fuel Loadings and the Role of Decomposition in Fine Fuel Accumulation, Journal of Advances in Modeling Earth Systems, 14, e2021MS002 818, https://doi.org/10.1029/2021MS002818, 2022.

Hantson, S., Arneth, A., Harrison, S. P., Kelley, D. I., Prentice, I. C., Rabin, S. S., Archibald, S., Mouillot, F., Arnold, S. R., Artaxo, P., Bachelet, D., Ciais, P., Forrest, M., Friedlingstein, P., Hickler, T., Kaplan, J. O., Kloster, S., Knorr, W., Lasslop, G., Li, F., Mangeon, S., Melton, J. R., Meyn, A., Sitch, S., Spessa, A., van der Werf, G. R., Voulgarakis, A., and Yue, C.: The status and challenge of global fire modelling, Biogeosciences, 13, 3359–3375, https://doi.org/10.5194/bg-13-3359-2016, 2016.

Hantson, S., Kelley, D. I., Arneth, A., Harrison, S. P., Archibald, S., Bachelet, D., Forrest, M., Hickler, T., Lasslop, G., Li, F., Mangeon, S., Melton, J. R., Nieradzik, L., Rabin, S. S., Prentice, I. C., Sheehan, T., Sitch, S., Teckentrup, L., Voulgarakis, A., and Yue, C.: Quantitative assessment of fire and vegetation properties in simulations with fire-enabled vegetation models from the Fire Model Intercomparison Project, Geoscientific Model Development, 13, 3299–3318, https://doi.org/10.5194/gmd-13-3299-2020, 2020.

Harper, K. L., Lamarche, C., Hartley, A., Peylin, P., Ottlé, C., Bastrikov, V., San Martín, R., Bohnenstengel, S. I., Kirches, G., Boettcher, M., Shevchuk, R., Brockmann, C., and Defourny, P.: A 29-year time series of annual 300 m resolution plant-functional-type maps for climate models, Earth System Science Data, 15, 1465–1499, https://doi.org/10.5194/essd-15-1465-2023, 2023.

Hess, P., Lange, S., Schötz, C., and Boers, N.: Deep Learning for Bias-Correcting CMIP6-Class Earth System Models, Earth's Future, 11, e2023EF004 002, https://doi.org/10.1029/2023EF004002, 2023.

Hua, W., Lou, S., Huang, X., Xue, L., Ding, K., Wang, Z., and Ding, A.: Diagnosing uncertainties in global biomass burning emission inventories and their impact on modeled air pollutants, Atmospheric Chemistry and Physics, 24, 6787–6807, https://doi.org/10.5194/acp-24-6787-2024, 2024.

Hussain, M. and Mahmud, I.: pyMannKendall: a python package for non parametric Mann Kendall family of trend tests., Journal of Open Source Software, 4, 1556, https://doi.org/10.21105/joss.01556, 2019.

Intergovernmental Panel on Climate Change (IPCC): Global Carbon and Other Biogeochemical Cycles and Feedbacks, Cambridge University Press, https://doi.org/10.1017/9781009157896.007, 2023.

Kaiser, J. W., Heil, A., Andreae, M. O., Benedetti, A., Chubarova, N., Jones, L., Morcrette, J.-J., Razinger, M., Schultz, M. G., Suttie, M., and van der Werf, G. R.: Biomass burning emissions estimated with a global fire assimilation system based on observed fire radiative power, Biogeosciences, 9, 527–554, https://doi.org/10.5194/bg-9-527-2012, 2012.

Kelley, D. I., Bistinas, I., Whitley, R., Burton, C., Marthews, T. R., and Dong, N.: How contemporary bioclimatic and human controls change global fire regimes, Nature Climate Change, 9, 690–696, https://doi.org/10.1038/s41558-019-0540-7, 2019.

Kim, H.-J., Kim, J.-S., Ham, Y.-G., Park, J.-H., Milodowski, D., Aragão, L. E. O. C., and Williams, M.: Anomalous temperature in North Tropical Atlantic linked to Brazilian Cerrado fires, npj Climate and Atmospheric Science, 8, 63, https://doi.org/10.1038/s41612-025-00945-w, 2025.

Kloster, S. and Lasslop, G.: Historical and future fire occurrence (1850 to 2100) simulated in CMIP5 Earth System Models, Global and Planetary Change, 150, 58–69, https://doi.org/10.1016/j.gloplacha.2016.12.017, 2017.

Kummu, M., Taka, M., and Guillaume, J. H. A.: Gridded global datasets for Gross Domestic Product and Human Development Index over 1990–2015, Scientific Data, 5, 180 004, https://doi.org/10.1038/sdata.2018.4, 2018.

Lasslop, G., Coppola, A. I., Voulgarakis, A., Yue, C., and Veraverbeke, S.: Influence of Fire on the Carbon Cycle and Climate, Current Climate Change Reports, 5, 112–123, https://doi.org/10.1007/s40641-019-00128-9, 2019.

Li, F., Levis, S., and Ward, D. S.: Quantifying the role of fire in the Earth system - Part 1: Improved global fire modeling in the Community Earth System Model (CESM1), Biogeosciences, 10, 2293–2314, https://doi.org/10.5194/bg-10-2293-2013, 2013.

Li, F., Val Martin, M., Andreae, M. O., Arneth, A., Hantson, S., Kaiser, J. W., Lasslop, G., Yue, C., Bachelet, D., Forrest, M., Kluzek, E., Liu, X., Mangeon, S., Melton, J. R., Ward, D. S., Darmenov, A., Hickler, T., Ichoku, C., Magi, B. I., Sitch, S., van der Werf, G. R., Wiedinmyer, C., and Rabin, S. S.: Historical (1700–2012) global multi-model estimates of the fire emissions from the Fire Modeling Intercomparison Project (FireMIP), Atmospheric Chemistry and Physics, 19, 12 545–12 567, https://doi.org/10.5194/acp-19-12545-2019, 2019.

Li, F., Song, X., Harrison, S. P., Marlon, J. R., Lin, Z., Leung, L. R., Schwinger, J., Marécal, V., Wang, S., Ward, D. S., Dong, X., Lee, H., Nieradzik, L., Rabin, S. S., and Séférian, R.: Evaluation of global fire simulations in CMIP6 Earth system models, Geoscientific Model Development, 17, 8751–8771, https://doi.org/10.5194/gmd-17-8751-2024, 2024.

Liu, T., Mickley, L. J., Marlier, M. E., DeFries, R. S., Khan, M. F., Latif, M. T., and Karambelas, A.: Diagnosing spatial biases and uncertainties in global fire emissions inventories: Indonesia as regional case study, Remote Sensing of Environment, 237, 111 557, https://doi.org/10.1016/j.rse.2019.111557, 2020.

Liu, Y., Fu, R., and Dickinson, R.: The Impacts of Smoke Aerosols on South American Monsoon, Bull. Amer. Meteor. Soc, 86, 1062–1063, 2005.

Liu, Z., Doherty, R. M., Wild, O., O'Connor, F. M., and Turnock, S. T.: Correcting ozone biases in a global chemistry–climate model: implications for future ozone, Atmospheric Chemistry and Physics, 22, 12 543–12 557, https://doi.org/10.5194/acp-22-12543-2022, 2022a.

Liu, Z., Eden, J. M., Dieppois, B., and Blackett, M.: A global view of observed changes in fire weather extremes: uncertainties and attribution to climate change, Climatic Change, 173, 14, https://doi.org/10.1007/s10584-022-03409-9, 2022b.

Liu, Z., Zhou, K., Yao, Q., and Reszka, P.: An interpretable machine learning model for predicting forest fire danger based on Bayesian optimization, Emergency Management Science and Technology, 4, https://doi.org/10.48130/emst-0024-0026, 2024.

Lundberg, S. M., Erion, G., Chen, H., DeGrave, A., Prutkin, J. M., Nair, B., Katz, R., Himmelfarb, J., Bansal, N., and Lee, S.-I.: From local explanations to global understanding with explainable AI for trees, Nature Machine Intelligence, 2, 2522–5839, https://doi.org/10.1038/s42256-019-0138-9, 2020.

Magahey, S. and Kooperman, G. J.: Isolating the effect of biomass burning aerosol emissions on 20th century hydroclimate in South America and Southeast Asia, Environmental Research Letters, 18, 104 029, https://doi.org/10.1088/1748-9326/acf7d4, 2023.

Mangeon, S., Voulgarakis, A., Gilham, R., Harper, A., Sitch, S., and Folberth, G.: INFERNO: a fire and emissions scheme for the UK Met Office's Unified Model, Geoscientific Model Development, 9, 2685–2700, https://doi.org/10.5194/gmd-9-2685-2016, 2016.

Marengo, J. A., Cunha, A. P., Cuartas, L. A., Leal, K. R. D., Broedel, E., Seluchi, M. E., Michelin, C. M., Baião, C. F. D. P., Angulo, E. C., Almeida, E. K., Kazmierczak, M. L., Mateus, N. P. A., Silva, R. C., and Bender, F.: Extreme Drought in the Brazilian Pantanal in 2019–2020: Characterization, Causes, and Impacts, Frontiers in Water, 3, https://doi.org/10.3389/frwa.2021.639204, 2021.

Marques, E. Q., Marimon-Junior, B. H., Marimon, B. S., Matricardi, E. A., Mews, H. A., and Colli, G. R.: Redefining the Cerrado–Amazonia transition: implications for conservation, Biodiversity and conservation, 29, 1501–1517, https://doi.org/10.1007/s10531-019-01720-z, 2020.

Mataveli, G., Pereira, G., Sanchez, A., de Oliveira, G., Jones, M. W., Freitas, S. R., and Aragão, L. E. O. C.: Updated Land Use and Land Cover Information Improves Biomass Burning Emission Estimates, Fire, 6, https://doi.org/10.3390/fire6110426, 2023.

Mathison, C., Burke, E., Hartley, A. J., Kelley, D. I., Burton, C., Robertson, E., Gedney, N., Williams, K., Wiltshire, A., Ellis, R. J., Sellar, A. A., and Jones, C. D.: Description and evaluation of the JULES-ES set-up for ISIMIP2b, Geoscientific Model Development, 16, 4249–4264, https://doi.org/10.5194/gmd-16-4249-2023, 2023.

Milare, G., Giarolla, A., and Escada, M. I. S.: Burned area occurrence in agrarian reform settlement projects in the Matopiba region, Brazil, Applied Geography, 166, 103 243, https://doi.org/10.1016/j.apgeog.2024.103243, 2024.

Naus, S., Domingues, L. G., Krol, M., Luijkx, I. T., Gatti, L. V., Miller, J. B., Gloor, E., Basu, S., Correia, C., Koren, G., Worden, H. M., Flemming, J., Pétron, G., and Peters, W.: Sixteen years of MOPITT satellite data strongly constrain Amazon CO fire emissions, Atmospheric Chemistry and Physics, 22, 14 735–14 750, https://doi.org/10.5194/acp-22-14735-2022, 2022.

Pacheco, P., Mo, K., Dudley, N., Shapiro, A., Aguilar-Amuchastegui, N., Ling, P., Anderson, C., and Marx, A.: Deforestation fronts: Drivers and responses in a changing world, Tech. rep., WWF, Gland, Switzerland, https://www.worldwildlife.org/documents/508/ocuoxmdil_Deforestation_fronts___drivers_and_responses_in_a_changing_world___f_3DJ6oVP.pdf, 2021.

Pedregosa, F., Varoquaux, G., Gramfort, A., Michel, V., Thirion, B., Grisel, O., Blondel, M., Prettenhofer, P., Weiss, R., Dubourg, V., Vanderplas, J., Passos, A., Cournapeau, D., Brucher, M., Perrot, M., and Duchesnay, E.: Scikit-learn: Machine Learning in Python, Journal of Machine Learning Research, 12, 2825–2830, https://doi.org/10.48550/arXiv.1201.0490, 2011.

Pereira, G., Longo, K. M., Freitas, S. R., Mataveli, G., Oliveira, V. J., Santos, P. R., Rodrigues, L. F., and Cardozo, F. S.: Improving the south America wildfires smoke estimates: Integration of polar-orbiting and geostationary satellite fire products in the Brazilian biomass burning emission model (3BEM), Atmospheric Environment, 273, 118 954, https://doi.org/10.1016/j.atmosenv.2022.118954, 2022.

Perktold, J., Seabold, S., Sheppard, K., ChadFulton, Shedden, K., jbrockmendel, j grana6, Quackenbush, P., Arel-Bundock, V., McKinney, W., Langmore, I., Baker, B., Gommers, R., yogabonito, s scherrer, Zhurko, Y., Brett, M., Giampieri, E., yl565, Millman, J., Hobson, P., Vincent, Roy, P., Augspurger, T., tvanzyl, alexbrc, Hartley, T., Perez, F., Tamiya, Y., and Halchenko, Y.: statsmodels/statsmodels: Release 0.14.2, https://doi.org/10.5281/zenodo.10984387, 2024.

Pope, R. J., Arnold, S. R., Chipperfield, M. P., Reddington, C. L. S., Butt, E. W., Keslake, T. D., Feng, W., Latter, B. G., Kerridge, B. J., Siddans, R., Rizzo, L., Artaxo, P., Sadiq, M., and Tai, A. P. K.: Substantial Increases in Eastern Amazon and Cerrado Biomass Burning-Sourced Tropospheric Ozone, Geophysical Research Letters, 47, e2019GL084 143, https://doi.org/10.1029/2019GL084143, 2020.

Power, J., Côté, M.-P., and Duchesne, T.: A Flexible Hierarchical Insurance Claims Model with Gradient Boosting and Copulas, North American Actuarial Journal, 28, 772–800, https://doi.org/10.1080/10920277.2023.2279782, 2024.

Rabin, S. S., Melton, J. R., Lasslop, G., Bachelet, D., Forrest, M., Hantson, S., Kaplan, J. O., Li, F., Mangeon, S., Ward, D. S., Yue, C., Arora, V. K., Hickler, T., Kloster, S., Knorr, W., Nieradzik, L., Spessa, A., Folberth, G. A., Sheehan, T., Voulgarakis, A., Kelley, D. I., Prentice, I. C., Sitch, S., Harrison, S., and Arneth, A.: The Fire Modeling Intercomparison Project (FireMIP), phase 1: experimental and

analytical protocols with detailed model descriptions, Geoscientific Model Development, 10, 1175–1197, https://doi.org/10.5194/gmd-10-1175-2017, 2017.

Rap, A., Spracklen, D. V., Mercado, L., Reddington, C. L., Haywood, J. M., Ellis, R. J., Phillips, O. L., Artaxo, P., Bonal, D., Restrepo Coupe, N., and Butt, N.: Fires increase Amazon forest productivity through increases in diffuse radiation, Geophysical Research Letters, 42, 4654–4662, https://doi.org/10.1002/2015GL063719, 2015.

Reddington, C. L., Morgan, W. T., Darbyshire, E., Brito, J., Coe, H., Artaxo, P., Scott, C. E., Marsham, J., and Spracklen, D. V.: Biomass burning aerosol over the Amazon: analysis of aircraft, surface and satellite observations using a global aerosol model, Atmospheric Chemistry and Physics, 19, 9125–9152, https://doi.org/10.5194/acp-19-9125-2019, 2019.

Rovithakis, A., Burke, E., Burton, C., Kasoar, M., Grillakis, M. G., Seiradakis, K. D., and Voulgarakis, A.: Estimating future wildfire burnt area over Greece using the JULES-INFERNO model, Natural Hazards and Earth System Sciences, 25, 3185–3200, https://doi.org/10.5194/nhess-25-3185-2025, 2025.

San Martín, R., Ottlé, C., and Sörensson, A.: Fires in the South American Chaco, from dry forests to wetlands: response to climate depends on land cover, Fire Ecology, 19, 57, https://doi.org/10.1186/s42408-023-00212-4, 2023.

Senf, F., Heinold, B., Kubin, A., Müller, J., Schrödner, R., and Tegen, I.: How the extreme 2019–2020 Australian wildfires affected global circulation and adjustments, Atmospheric Chemistry and Physics, 23, 8939–8958, https://doi.org/10.5194/acp-23-8939-2023, 2023.

Silva-Junior, C. H. L., Buna, A. T. M., Bezerra, D. S., Costa, O. S., Santos, A. L., Basson, L. O. D., Santos, A. L. S., Alvarado, S. T., Almeida, C. T., Freire, A. T. G., Rousseau, G. X., Celentano, D., Silva, F. B., Pinheiro, M. S. S., Amaral, S., Kampel, M., Vedovato, L. B., Anderson, L. O., and Aragão, L. E. O. C.: Forest Fragmentation and Fires in the Eastern Brazilian Amazon–Maranhão State, Brazil, Fire, 5, https://doi.org/10.3390/fire5030077, 2022.

Snyder, P. K.: The Influence of Tropical Deforestation on the Northern Hemisphere Climate by Atmospheric Teleconnections, Earth Interactions, 14, 1 – 34, https://doi.org/10.1175/2010EI280.1, 2010.

Teckentrup, L., Harrison, S. P., Hantson, S., Heil, A., Melton, J. R., Forrest, M., Li, F., Yue, C., Arneth, A., Hickler, T., Sitch, S., and Lasslop, G.: Response of simulated burned area to historical changes in environmental and anthropogenic factors: a comparison of seven fire models, Biogeosciences, 16, 3883–3910, https://doi.org/10.5194/bg-16-3883-2019, 2019.

Teixeira, J. C., Folberth, G. A., O'Connor, F. M., Unger, N., and Voulgarakis, A.: Coupling interactive fire with atmospheric composition and climate in the UK Earth System Model, Geoscientific Model Development, 14, 6515–6539, https://doi.org/10.5194/gmd-14-6515-2021, 2021.

Thornhill, G. D., Ryder, C. L., Highwood, E. J., Shaffrey, L. C., and Johnson, B. T.: The effect of South American biomass burning aerosol emissions on the regional climate, Atmospheric Chemistry and Physics, 18, 5321–5342, https://doi.org/10.5194/acp-18-5321-2018, 2018.

van der Werf, G. R., Randerson, J. T., Giglio, L., Collatz, G. J., Mu, M., Kasibhatla, P. S., Morton, D. C., DeFries, R. S., Jin, Y., and van Leeuwen, T. T.: Global fire emissions and the contribution of deforestation, savanna, forest, agricultural, and peat fires (1997–2009), Atmospheric Chemistry and Physics, 10, 11 707–11 735, https://doi.org/10.5194/acp-10-11707-2010, 2010.

van der Werf, G. R., Randerson, J. T., Giglio, L., van Leeuwen, T. T., Chen, Y., Rogers, B. M., Mu, M., van Marle, M. J. E., Morton, D. C., Collatz, G. J., Yokelson, R. J., and Kasibhatla, P. S.: Global fire emissions estimates during 1997–2016, Earth System Science Data, 9, 697–720, https://doi.org/10.5194/essd-9-697-2017, 2017.

van Leeuwen, T. T., van der Werf, G. R., Hoffmann, A. A., Detmers, R. G., Rücker, G., French, N. H. F., Archibald, S., Carvalho Jr., J. A., Cook, G. D., de Groot, W. J., Hély, C., Kasischke, E. S., Kloster, S., McCarty, J. L., Pettinari, M. L., Savadogo, P., Alvarado, E. C.,

Boschetti, L., Manuri, S., Meyer, C. P., Siegert, F., Trollope, L. A., and Trollope, W. S. W.: Biomass burning fuel consumption rates: a field measurement database, Biogeosciences, 11, 7305–7329, https://doi.org/10.5194/bg-11-7305-2014, 2014.

van Marle, M. J. E., Kloster, S., Magi, B. I., Marlon, J. R., Daniau, A.-L., Field, R. D., Arneth, A., Forrest, M., Hantson, S., Kehrwald, N. M., Knorr, W., Lasslop, G., Li, F., Mangeon, S., Yue, C., Kaiser, J. W., and van der Werf, G. R.: Historic global biomass burning emissions for CMIP6 (BB4CMIP) based on merging satellite observations with proxies and fire models (1750–2015), Geoscientific Model Development, 10, 3329–3357, https://doi.org/10.5194/gmd-10-3329-2017, 2017.

Velásquez-García, M. P., Pope, R. J., and Turnock, S.: South America CO emissions simulated by INFERNO fire models and model sensitivity analysis from 2004 to 2021, https://doi.org/10.5281/zenodo.18337852, 2026.

Vinodkumar, V., Dharssi, I., Yebra, M., and Fox-Hughes, P.: Continental-scale prediction of live fuel moisture content using soil moisture information, Agricultural and Forest Meteorology, 307, 108 503, https://doi.org/10.1016/j.agrformet.2021.108503, 2021.

Volkholz, J. and Ostberg, S.: ISIMIP3a landuse input data, https://doi.org/10.48364/ISIMIP.571261.1, 2022.

Wang, S., Foster, A., Lenz, E. A., Kessler, J. D., Stroeve, J. C., Anderson, L. O., Turetsky, M., Betts, R., Zou, S., Liu, W., Boos, W. R., and Hausfather, Z.: Mechanisms and Impacts of Earth System Tipping Elements, Reviews of Geophysics, 61, e2021RG000 757, https://doi.org/10.1029/2021RG000757, 2023a.

Wang, S. S.-C., Qian, Y., Leung, L. R., and Zhang, Y.: Interpreting machine learning prediction of fire emissions and comparison with FireMIP process-based models, Atmospheric Chemistry and Physics, 22, 3445–3468, https://doi.org/10.5194/acp-22-3445-2022, 2022.

Wang, S. S.-C., Leung, L. R., and Qian, Y.: Projection of Future Fire Emissions Over the Contiguous US Using Explainable Artificial Intelligence and CMIP6 Models, Journal of Geophysical Research: Atmospheres, 128, e2023JD039 154, https://doi.org/10.1029/2023JD039154, 2023b.

Wiltshire, A. J., Duran Rojas, M. C., Edwards, J. M., Gedney, N., Harper, A. B., Hartley, A. J., Hendry, M. A., Robertson, E., and Smout-Day, K.: JULES-GL7: the Global Land configuration of the Joint UK Land Environment Simulator version 7.0 and 7.2, Geoscientific Model Development, 13, 483–505, https://doi.org/10.5194/gmd-13-483-2020, 2020.

Wu, L., Su, H., and Jiang, J. H.: Regional simulations of deep convection and biomass burning over South America: 2. Biomass burning aerosol effects on clouds and precipitation, Journal of Geophysical Research: Atmospheres, 116, https://doi.org/10.1029/2011JD016106, 2011.

Zhou, Y., Yan, H., and Luo, J.-J.: Impacts of Amazon fire aerosols on the subseasonal circulations of the mid-high latitudes, Frontiers in Earth Science, 8, 609 554, https://doi.org/10.3389/feart.2020.609554, 2020.